ENVIRONMENTALLY RESPONSIVE LIPOSOMES

FOR TREATMENT OF

METASTATIC TRIPLE NEGATIVE BREAST CANCER

By

SALLY STRAS

A dissertation submitted to the

School of Graduate Studies

Rutgers, The State University of New Jersey

In partial fulfillment of the requirements

For the degree of

Doctor of Philosophy

Graduate Program in Chemical and Biochemical Engineering

Written under the direction of

Stavroula Sofou

And approved by

_____

_____

_____

_____

New Brunswick, New Jersey

May 2018

ABSTRACT OF THE DISSERTATION

Environmentally Responsive Liposomes

For Treatment of

Metastatic Triple Negative Breast Cancer

By SARAH (SALLY) STRAS

Dissertation Director:

Stavroula Sofou

In 2015, it was estimated that approximately 1.7 million women were diagnosed with breast cancer in the United States alone. Breast cancer is the most common cancer among women. One in eight women in their lifetime will have to endure the tribulations of discovering that they have breast cancer and all that comes in hopes of beating the disease. Triple-negative breast cancer (TNBC) is a subgroup of breast cancer associated with a poor prognosis and a higher chance of cancer metastasis outside the breast. TNBC is defined as being negative in gene expression for estrogen receptor (ER), progesterone receptor (PR) and lacking gene expression of HER2/neu. Current methods for targeting TNBC tumors remain in investigative stages due to the difficulty in discovering an appropriate and direct method of targeting. To enable selective and effective treatment of TNBC solid tumors, we study a drug delivery carrier of cisplatin (CDDP) - a clinically accepted major line of therapy for TNBC - that is designed to ultimately result in (a) deep penetration and homogeneous distribution of the drug within tumors and (b) enhanced

uptake by the cancer cells that constitute these tumors. Towards these aims, we engineered a carrier that is a tunable (pH-sensitive) liposome encapsulating cisplatin. These liposomes are designed to form lipid-phase separated domains at acidic pH. Domain formation is tuned to trigger content release, and the change is pH is used to increase the adsorptive/adhesive property of these liposomes. Improved tumor penetration of delivered cisplatin is expected to be achieved by triggered release of cisplatin directly within the tumor interstitial region from extravasated liposomes. Further increase in intracellularly delivered cisplatin (due to more favorable retention of liposomes by solid tumors *in vivo*) is expected to be achieved by liposomes that are functionalized with an adhesive switch on their surface with the aim to slow their clearance from the tumor.

ACKNOWLEDGEMENTS

I would first like to thank my dissertation advisor Dr. Stavroula Sofou. Because of her leadership and constant availability, I have been able to produce a substantial amount of publishable work. No matter what time or day she was always there to answer a question or help solve a problem and for that I am grateful. Thank you for molding me into a scientist extremely confident in my abilities. I would also like to thank my committee members: Dr. Charles Roth, Dr. Martin Yarmush, Dr. Prabhas Moghe and Dr. Yannis Kevrekidis for their time and constructive criticism to make this project stronger and more scientifically sound.

I would also like to acknowledge fellow members of the Sofou lab, both past and present- going through this program wouldn't have been possible without support from them. They include Dr. Charles Zhu, Dr. Michelle Sempkowski, Ms. Alaina Howe and Mr. Aprameya Prasad. The Starbucks runs, lunches and dinners out provided much needed time to laugh and take a break and I feel lucky to have had all of you as a support system throughout my PhD research.

I'd like to acknowledge my family: my brother and sister for listening to my rants about my experiments and mice, and for accepting the fact that I couldn't always visit because of my schedule (You'll be seeing a lot more of me now!) My Mom- she taught me, from her example, to be strong and independent and that women can excel in math and science and always encouraged me to be great (You won't have to ask me how my spheroids are anymore!). My Dad- throughout this experience he has listened to every concern and problem whether it was social, scientific, or pertaining to my next career steps, and he *always* had good advice and made me feel calmer after speaking with him.

I'd like to acknowledge my boyfriend, Anthony Calvano, who always has my back, sometimes more than I have my own. Even with the relocation to Baltimore, he was still able to support me from a far and I could not have completed this without his unmatched support and love. And to his family, for becoming my second family and for treating me like one of their own- the vacations and dinners provided a time to relax and enjoy myself in the midst of a stressful PhD; I cannot thank them enough.

I would like to thank the following funding sources- this research was partially supported by the American Cancer Society Research Scholar Grant RSG-12-044-01, the National Science Foundation grant CBET 1510015, and a grant from the Elsa U. Pardee Foundation. Special acknowledgements to the High Resolution Microscopy Facility, Department of Biomedical Engineering, Rutgers University as well as Desmond Jacobs at the Molecular Imaging Facility at Johns Hopkins University. I'd also like to acknowledge members of the Histopathology department at Johns Hopkins University, specifically Nadine Forbes and Dr. Cory Brayton.

TABLE OF CONTENTS

LIST OF FIGURES

LIST OF TABLES

CHAPTER 1: INTRODUCTION

1.1: Triple Negative Breast Cancer

In women, 29% of all cancer cases are breast cancer, which makes it the most common cancer among women [1]. Of all cases, 10-17% are considered to be triple negative breast cancer (TNBC) [1]. Triple negative breast cancer is defined as being estrogen receptor (ER) negative, progesterone receptor (PR) negative, and lacking in HER2 expression [2, 3].TNBC patients have the lowest 5-year survival rates among all breast cancer patients [4]. In advanced solid tumors, including Triple Negative Breast Cancer (TNBC) tumors, the heterogeneous distribution of therapeutics to all regions of tumors limits efficacy [5, 6]. TNBCs, in particular, are associated with poor prognosis due to high proliferation and recurrence outside the breast [3, 7] combined with lack of effective therapeutic modalities [8]. Some recently developed treatments include inhibitions of various genes including PARP, EGFR and MEK, as well as p53 signaling modulation [3, 4]. Platinum agents have been a popular choice of treatment due to the sensitivity of the disease to the drug, which has been determined in several studies [4, 8].

1.3: Current Clinical Liposomal Cisplatin

Results from the clinic do show the sensitivity of TNBC to DNA-damaging platinum-based compounds [9], which is the basis for increased clinical use of platinum-derived agents [3, 10]. However, the debilitating toxicities of platinum compounds [11, 12] have given rise to liposomal formulations of cisplatin with some currently being clinically explored [5, 13]. The reported liposomal cisplatin approaches, however, are

not designed to directly address the heterogeneous distributions and limited penetration of the nanometer-sized carriers and/or of their therapeutic contents within solid tumors [5, 13]. Several formulations have made it to the clinical level with little to moderate success. SPI-77 was developed as a non-environmentally responsive liposome encapsulating cisplatin. It made it to Phase II clinical trials to evaluate its efficacy for treating non-small-cell lung cancer (NSCLC). While no significant toxicities were noted, treatment with SPI-77 only led to 'modest activity' in patients [14]. Lipoplatin^{TM} is the most notable liposomal form of cisplatin in the clinic. It is in several different Phases of clinical trials for several types of cancers including breast cancer, gastrointestinal cancer, and a Phase III trial for NSCLC. The formulation allows for significant tumor uptake and compared to administration of free cisplatin toxicities are greatly reduced [15, 16].

1.4: Dissertation Summary

To advance selectivity and efficacy in treatment of TNBC solid tumors, we study a lipid-based nanometer-sized carrier of cisplatin that is designed with the aim to improve drug penetration and to decrease heterogeneities of the drug's distribution within the tumor interstitium. The carrier is a pH-releasing liposome encapsulating cisplatin. Tumor selective uptake by these liposomes is expected to be mediated by the EPR effect [17, 18]. Improvement in efficacy is designed to be mediated by the pH-triggered release of cisplatin within the tumor interstitium ($7.0 < pH < 6.4$) [19, 20] by extravasated liposomes [21]. Fast and extensive release of cisplatin from liposomes in the tumor interstitium are expected to (1) enhance the '(bio)availability' of delivered cisplatin which will be free to diffuse across the cancer cell membranes, and to (2) improve cisplatin's

intratumoral distribution due to the small size of released cisplatin which should exhibit greater diffusivities within the interstitial space relative to the nanometer-sized carrier.

To further enhance uptake of cisplatin by cancer cells by delaying liposome clearance from solid tumors *in vivo*, we functionalized the pH-releasing liposomes. These sticky liposomes *were designed to* electrostatically bind to (but not significantly get internalized by) cells when exposed to an acidic environment (pH 6.8-6.5). This allowed the liposomes to selectively bind to the extracellular matrix and the cancer cells in the tumor interstitium while exhibiting minimal cell internalization.

Liposome design: In this study, the pH-tunable liposome membranes were designed to form phase-separated lipid domains at the pH of the tumor interstitum. Liposome bilayers contained two types of lipid: non-titratable lipids and titratable domain-forming lipids [22]. Domain formation is dependent on the extent of ionization of the headgroups of the domain-forming lipids which is controlled by the pH. Therefore, pH can be used to shift the balance between electrostatic repulsions and H-bonding attractions among the titratable lipids [23]. In particular, at neutral pH, the headgroups of the domain forming lipids are negatively-charged, opposing close approximation of lipids resulting in homogenous distribution of each lipid type throughout the lipid membrane. As the pH is decreased, gradual headgroup protonation minimizes the electrostatic repulsions, and lipid phase-separated domains are formed driven mostly by H-bonding.

The property of pH-activated content release is enabled by engineering the interfaces to have defects between the phase-separated lipid domains to allow for increased membrane permeability. This is achieved by choosing, for the formation of the liposome membrane, both types of lipids to be in the *gel-phase* and with *different* acyl-

tail lengths; our group has previously proposed that the differences in acyl-tail lengths at the domain interface control the extent of molecular defects in lipid packing within the internal hydrophobic space within the bilayer [22].

The property of pH-activated adhesion was enabled by the addition of a titratable lipid that becomes positively charged at acidic pH - the pH of the tumor interstitium. The titratable head group was designed to be located at the end of PEG chains on liposomes allowing for interaction with negatively charged areas of the extracellular matrix and with areas rich in negatively charged lipids on cell plasma membranes. Importantly, the location of the positive charge on the edge of the labile PEG corona on the surface of these liposomes was hypothesized to prevent exchange of lipids from the cell plasma outer lipid leaflet with the lipids of the cell adsorbed liposomes resulting in lower extents of liposome fusion with the plasma membrane and potentially in lower extents of internalization of electrostatically cell adsorbed liposomes .

In this study, we evaluated the pH-sensitive release of cisplatin from liposomes in the acidic environment of the tumor interstium ($7.0 < pH < 6.5$) with the aim to improve the diffusion-limited transport of cisplatin within solid tumors.

To test the pH-sensitive liposomal constructs, three Specific Aims were evaluated in which the pH-releasing adhesive liposomes encapsulating cisplatin were compared to pH-releasing non-adhesive liposomes, Lipoplatin analogues (non-pH-releasing and non-adhesive liposomal cisplatin) and to free cisplatin:

Specific Aim 1.) To design liposomes loaded with cisplatin with a built-in triggered release mechanism to release cisplatin into the interstitial space of TNBC tumor analogues.

Specific Aim 2.) To develop liposomes containing the adhesive switch loaded with cisplatin with built-in triggered release.

Specific Aim 3.) To evaluate the efficacy of pH-releasing and adhesive liposomal cisplatin to suppress the growth of TNBC metastases in a TNBC orthotopic mouse model with lung, liver and lymph node metastases.

In Chapter 2 we designed and characterized pH-releasing liposomes loaded with cisplatin that retained contents in neutral pH and released contents in acidic pH (pH 6.5-6.0). We compared their efficacy *in vitro* to free cisplatin and to non-pH-releasing liposomes. Their efficacy was evaluated on TNBC cell monolayers, and 3D multicellular spheroids that mimic the avascular region of tumors. The triggered release caused by the drop in pH in the tumor interstitium led to enhanced efficacy of the pH-releasing liposomes, compared to the aforementioned controls, on TNBC monolayers and multicellular spheroids.

Chapter 3 involved key optimization of the liposomal composition to enable slower clearance of the liposome from the tumor and therefore to result in increased time integrated doses within the tumors. It is important to develop a liposome with the best chances of success in an animal model and that success lies in greater amounts of bioavailable cisplatin at the tumor site. Liposomes were functionalized with the electrostatic adhesive switch in addition to the property of content release in the tumor interstitium.

To determine if these liposomes were able to surpass the liposomes evaluated in Chapter 2 in terms of efficacy, similar experiments were conducted *in vitro* comparing

the previously developed liposomes, the adhesive liposomes, non-pH-releasing liposomes (with and without the adhesive switch) and free cisplatin. Results here indicated better efficacy on TNBC tumor surrogates when the adhesion switch was incorporated in the pH-releasing liposome membrane. The next steps were to see if the liposomes could potentially be effective *in vivo* and the all above mentioned constructs were tested in an orthotopic xenograft mouse model. The mouse model was used to determine the efficacy of the developed liposomes, as well as appropriate controls, on metastatic, triple negative breast cancer. Results showed the ability of the pH-releasing liposomes with the adhesion switch to slow the kinetics of metastatic growth. However, there were no significant differences in survival of any of the groups treated with liposomal constructs and the no treatment group due to the particularly aggressive character of the tumor model as compared to the treatment schedule and intrinsic killing efficacy of chosen chemotherapy.

CHAPTER 2: INTERSTITIAL RELEASE OF CISPLATIN FROM TRIGGERABLE LIPOSOMES ENHANCES EFFICACY AGAINST TRIPLE NEGATIVE BREAST CANCER SOLID TUMOR ANALOGUES

Note: data in this chapter was adapted from the following manuscript which is published: **Stras, S**; Holleran, T; Howe, A; Sofou, S. "Interstitial Release of Cisplatin from Triggerable Liposomes Enhances Efficacy Against Triple Negative Breast Cancer Solid Tumor Analogues" *Molecular Pharmaceutics*. 2016, 13(9), 3224- 3233.

2.1: Introduction

In advanced solid tumors, including Triple Negative Breast Cancer (TNBC) tumors, the heterogeneous distribution of therapeutics limits efficacy [6, 24] TNBCs, in particular, are associated with poor prognosis due to high proliferation and recurrence outside the breast [3, 7] combined with lack of effective therapeutic modalities [8] TNBC is defined as being negative in gene expression for the estrogen, progesterone, and HER2/neu receptors [3] and encompasses a particularly heterogeneous group of tumors which account for 15 - 23 % of invasive breast carcinomas with the lowest 5-year survival rates among all breast cancer patients[4].

TNBC may exhibit sensitivity to DNA-damaging platinum-based compounds [9], which is the basis for increased clinical use of platinum-derived agents [3, 10]. However, the debilitating toxicities of platinum compounds [11, 12] have given rise to liposomal formulations of cisplatin with some currently being clinically explored [5, 13]. The reported liposomal cisplatin approaches, however, are not designed to directly address the

heterogeneous distributions and limited penetration of the nanometer-sized carriers and/or of their therapeutic contents within solid tumors [5, 13].

To advance selectivity and efficacy in treatment of TNBC solid tumors, we study a lipid-based nanometer-sized carrier of cisplatin that is designed with the aim to improve drug penetration within the tumor interstitium. The carrier is a pH-releasing liposome loaded with cisplatin. Tumor selective uptake by these liposomes is expected to be mediated by the EPR effect [17, 18] Improvement in efficacy is designed to be mediated by the pH-triggered release of cisplatin within the tumor interstitium ($7.0 > pH \geq 6.0$) [19, 20] by extravasated liposomes [22]. Fast and extensive release of cisplatin from liposomes in the tumor interstitium are expected to (1) improve cisplatin's intratumoral distribution due to the small size of released cisplatin which should exhibit greater diffusivities within the interstitial space relative to the nanometer-sized carrier, and to (2) enhance the '(bio)availability' of delivered cisplatin which will be free to diffuse across the cancer cell membranes. The pH-releasing liposomes are used, in other words, as drug depots which release cisplatin significantly more rapidly and extensively than conventional, non-pH-releasing liposomes.

The utilization of pH-sensitivity in cisplatin's release from liposomes has been reported for the acidic pH in endosomes ($pH \sim 5.5$) following liposomal internalization by cells [5]. In the present study, however, we evaluate the pH-sensitive release of cisplatin from liposomes in the less acidic pH of the tumor interstium ($7.0 < pH \leq 6.0$) with the aim to primarily improve the intratumoral penetration of free cisplatin.

In this study, the pH-releasing liposome membranes are designed to form phase-separated lipid domains at the pH of the tumor interstitum. We have previously described

these liposome membranes which primarily contain two lipid types: one with a non-titratable headgroup and one with a titratable domain-forming headgroup [21, 22]. We demonstrated that the extent of ionization on the headgroups of the domain-forming lipids is controlled by the pH which can be used to shift the balance between electrostatic repulsions and H-bonding attractions [23]. In particular, at neutral pH, the headgroups of the domain forming lipids are negatively-charged, opposing close proximity between lipids, resulting in uniform lipid membranes. As the pH is decreased, at pH values relevant to the tumor interstitium, gradual headgroup protonation minimizes the electrostatic repulsion, and lipid domains are formed driven mostly by H-bonding. Phase separation is reversible with pH [25].

We have shown that domain formation alone is necessary but not sufficient to result in increased membrane permeability [22]. The property of pH-activated content release is enabled by engineering the boundaries of the phase-separated lipid domains to form extensive defects in lipid packing resulting in increased membrane permeability. This is achieved by choosing the above both types of lipids to be in the *gel-phase* with *different* acyl-tail lengths[22]. In the present study, the pH-releasing liposomes contain lipid pairs with different acyl-tail lengths, and the non-pH-releasing liposomes comprise lipid constituents all with identical acyl-tail lengths.

In this study, we aim to assess the role of cisplatin's intratumoral distributions on controlling growth by evaluating liposomes with pH-triggered release of encapsulated cisplatin, and by comparing their efficacy to non-pH-releasing liposomal cisplatin and free (not liposomal) cisplatin on TNBC cells with different sensitivities to cisplatin (MDA-MB-231 and MDA-MB-468) in monolayers and in 3-dimensional multicellular

spheroids. To evaluate the role of limited penetration-depth profiles of liposomes and therapeutic agents, [6, 26-28] we utilized multicellular spheroids as surrogates of the avascular regions of solid tumors [26]. The 3-D structure of multicellular spheroids affects diffusion of the carriers and drugs in addition to nutrients, therefore, causing changes in spheroid physiology and other relevant properties such as pH-gradients.

2.2: Materials and Methods

Materials

All lipids were obtained from Avanti Polar lipids (Alabaster, USA) and included 1,2-distearoyl-sn-glycero-3-phosphocoline (DSPC), 2-dihenarachidoyl-sn-glycero-3-phosphocoline (21PC), 1,2-dioctadecanoyl-*sn*-glycero-3-phospho-L-serine (sodium salt) (DSPS), 1,2-distearoyl-sn-glycero-3-phosphoethanolamine-N-[amino(polyethylene glycol)-2000](ammonium salt) (DSPE-PEG), and 1,2-dipalmitoyl-sn-glycero-3-phosphoethanolamine-N-(Lissamine Rhodamine B Sulfonyl) (Ammonium Salt) (Rhodamine-lipid). Cholesterol , cis-diamminedichloroplatinum (II) (cisplatin), phosphate buffered saline (PBS) tablets, Sephadex G-50 resin, Sepharose 4B resin, and chloroform were purchased from Sigma–Aldrich Chemical (Atlanta, GA). Polycarbonate membranes (100 nm pore size) for extrusion were purchased from Avestin (Ottawa, ON, Canada). Ethylenediaminetetraacetic Acid (EDTA), as well as Carboxyfluorescein diacetate succinimidyl ester (CFDA SE) were purchased from ThermoFisher Scientific (Waltham, MA). Quant-it DSDNA Assay Kit and Purelink Genomic DNA kit were purchased from Life Technologies (Carlsbad, CA).

Cell Lines

MDA-MB-468 and MDA-MB-231 human breast cancer cell lines were obtained from the American Type Culture Collection (ATCC, Rockville, MC, USA). MDA-MB-231 cells were cultured in EMEM Media supplemented with 10% fetal bovine serum and 100 units/mL penicillin and 100 µg/mL streptomycin solution at 37°C with 5% CO_2. MDA-MB-468 cells were cultured in L15 Media supplemented with 10% fetal bovine serum and 1% penicillin streptomycin 100x solution at 37°C in 100% air. Media was purchased from ATCC, fetal bovine serum was purchased from Omega Scientific (Tarzana, CA), and penicillin streptomycin and Matrigel™ were from Corning Life Sciences (Corning, NY).

Liposome Preparation, Characterization, and Loading of Cisplatin

The pH-releasing liposomes were composed of 21PC:DSPS:Cholesterol:DSPE-PEG at a 0.60:0.20:0.10:0.10 mole ratio, and the non-pH-releasing liposomes were composed of DSPC:DSPS:Cholesterol:DSPE-PEG at a 0.55:0.18:0.17:0.09 mole ratio. Both compositions were labeled with 0.125 mole % Rhodamine-lipid. All lipids were dissolved in chloroform, or a mixture of chloroform and methanol, and liposomes were prepared using the thin film hydration method [22]. Briefly, lipids (80 µmol total lipid) were dried using a Buchi Rotavapor under vacuum at 60°C, followed by exposure to a stream of Nitrogen for 5 minutes. Then, 1 mL of PBS (containing 1 mM EDTA) at pH 7.4 was added to the film and the suspension was annealed at 60°C for 2 hours followed by extrusion through two stacked 100 nm sized polycarbonate membranes 21 times at a temperature at least 10°C above the highest transition temperature of constituent lipids. EDTA was added to chelate any potential calcium or other multivalent cations which

may have been present in the water phase that was used to hydrate lipids. Following extrusion, the liposome suspension was run through a Sepharose 4B column, eluted in PBS at pH 7.4, to separate the liposomes from any micelles formed during the annealing process. An aliquot of the collected liposome fraction was then loaded with cisplatin using the passive equilibration method [29]. Briefly, liposomes (30 mM lipid) were pre-warmed at 80°C, and were then added to cisplatin powder to obtain a cisplatin concentration of 17 mg/mL, which was previously determined as the solubility limit of cisplatin at 80°C [29]. This suspension was then gently mixed for 4 hours at 80°C, and, upon completion of incubation, the suspension was cooled to room temperature and the insoluble cisplatin was pelleted by centrifugation at 1000 x g for 3 minutes. (The heating treatment did not result in measureable changes/degradation of lipids as shown in Figures A.1 and A.2 in the Appendix.) Non-encapsulated cisplatin was removed by a Sephadex G50 column of the supernatant eluted with PBS at pH 7.4.

An aliquot of the collected liposome fraction was diluted in 10% (v/v) HCl, and the platinum content was measured using a Graphite Furnace Atomic Absorption (GFAAS) Spectrometer (Buck Scientific, Norwalk, CT) at 265.9 nm. Before quantitation of cisplatin, a Pt calibration curve was performed using Pt standards. Also, the possible effects on Pt measurement of lipid content, of cells or of other components in the measured samples were evaluated. None of the above were found to affect the Pt signal. Lipid concentrations were evaluated using the Stewart's Assay [30]. Briefly, to determine the lipid concentration, a fraction of the liposome suspension was frozen and lyophilized. When dried, the samples were re-suspended in 2 mL of chloroform, and then 1 mL of thiocyanate reagent (27 g/L ferric chloride and 20 g/L ammonium thiocyanate) was added

and samples were shaken for 30 seconds. After shaking, samples were diluted further in chloroform, and absorbance at 488 nm was measured on a spectrophotometer. To obtain a calibration curve with the Stewart's Assay, known amounts of lipid mixtures (as the liposome compositions used in this study) were processed in the same way as above, and the measured absorbance was correlated to known lipid concentrations. The liposome suspensions were then sterilized using a 0.2 µm polyether sulfone filter (GE Life Sciences, Pittsburgh, PA). Size distributions of liposome suspensions and zeta potential were measured using a Malvern Zetasizer ZS90 (Malvern Instruments, Malvern, UK).

In Vitro Cisplatin Release Assay

Liposomes were added to EMEM cell culture media at different pH values at a final lipid concentration of 1 mg/mL. After a 6- hour incubation at 37°C, a 1 mL aliquot was removed and was ran through a Sephadex G50 column to separate liposomes from released cisplatin. To ensure that no cisplatin was being released from liposomes during the G50 column separation, the eluted PBS buffer was chosen to be at pH 7.4 at which pH liposomes are not designed to release their contents. To ensure that no cisplatin was being lost in the G50 column during elution, all fractions were collected and the mass balance of cisplatin was confirmed to be closed. A portion of the liposome fraction eluted from the column was diluted in 10% HCl and the cisplatin content was measured using the GFAAS. The concentration of cisplatin associated with liposomes after incubation was compared to the cisplatin concentration initially associated with liposomes to obtain a percent of cisplatin retained over the course of incubation.

Viability studies on cell monolayers

Cells were trypsinized and plated on 96-well plates at a density of 30,000 cells per well and were incubated at 37°C for 6 and 24 hours with both types of liposomal cisplatin, with not loaded liposomes, and with the free cisplatin at a range of concentrations and at extracellular pH values of 7.4, 6.5 and 6.0. Upon completion of incubation, cells were washed twice with sterile PBS, and fresh cell culture media was added to cells which were then allowed to grow for two doubling times (55 and 35 hours for MDA-MB-468 and MDA-MB-231, respectively) before being analyzed for cell viability using an MTT Assay. Percent cell viabilities were normalized relative to the measured cell viabilities of cells that did not receive treatment at the same extracellular pH values. Acidification of the extracellular pH did not decrease cell viability by more than 7-8 % relative to physiologic pH (Figure A.3).

To measure the amount of cisplatin uptake per cell in the above incubation conditions, cells were platted on 12-well plates at a density of 300,000 cells per well. Treatment was added to monolayers as above. After the incubation period, cells were trypsinized and washed. After centrifugation, cells were re-suspended in 200 μL of DI water and were prepared for GFAAS measurement by sonication for 10 minutes, and a subsequent addition of 20 μL of Triton X-100 to ensure cell lysis. The supernatant of cells, during centrifugation cycles, was used to determine the retention of cisplatin by liposomes using size exclusion chromatography as described above.

To determine the amount of cisplatin bound to nuclear DNA in the above incubation conditions, cells were plated at a density of 1 million cells per well in a 6-well plate. Free cisplatin and liposomal cisplatin were added at several concentrations for 24

hours. Upon completion of incubation, cells were washed with sterile PBS, were trypsinized, were centrifuged, and were then re-suspended in 0.2 mL of PBS. A 10 µL aliquot was taken to count the cell number, and DNA purification was performed using the Purelink Genomic DNA kit following the protocol for Mammalian Cells according to manufacturer's instructions (Life Technologies, Carlsbad, CA). Briefly, extracted DNA was eluted in 80 µL, and an aliquot was diluted in pH 8.0 10 mM Tris-HCl to measure the DNA concentration using the Quant-it DSDNA Assay Kit (Life Technologies, Carlsbad, CA). The remaining DNA was concentrated by lyophilization and measured on the GFAAS for cisplatin content.

Spheroid Formation and Characterization

Spheroids were formed first by trypsinizing confluent 225 cm^2 flasks of cells and diluting the cells to a concentration of 1000 cells per mL. The following steps were performed on ice: Matrigel™ was added to the cell suspension at a concentration of 2.5% (v/v) to promote cell-cell adhesion [31]. Cells were plated onto U-shaped 96-well plates treated with poly-HEMA (to minimize cell adhesion on the plates [31]) and centrifuged at 1000 RCF for 10 minutes at 4°C. Then, the plates were placed in an incubator (5% CO_2 at 37°C) and the spheroids grew until they reached the desired size of ~ 300 µm in diameter.

Only MDA-MB-468 spheroids, unlike the monolayers, were cultured in RPMI-1640 (supplemented with 10% FBS, 100 units/mL penicillin and 100 µg/mL) streptomycin at 37°C with 5% CO_2. To enable stable spheroid transfer upon reaching the desired size, spheroids were grown in spheroid-conditioned media (SCM) which was

removed from wells that spheroids had been growing in for approximately two weeks in the absence of treatment.

The spheroid interstitial pH gradient was measured using SNARF-4F, a cell impermeant pH-sensitive fluorophore. Spheroids were incubated with SNARF-4F at a concentration of 200 μM for 12 hours. Then, the spheroids were washed in a well of fresh media and placed in 96-well flat bottom plates with fresh media for confocal imaging. Z-stack images were taken on a Leica Confocal Microscope TCS SP2 at a 10x air objective. The calibration curve was developed by imaging free SNARF-4F in wells containing media (20 μM) of known pH in the range of interest (7.4 - 6.3) with 2.5% v/v Matrigel as to mimic the spheroid environment, and by plotting the ratio of the fluorescence intensities at the emission wavelengths 580 nm over 640 nm (ex: 543 nm) vs. the known pH values upon correction of images for background fluorescence. Radially averaged intensities within spheroids were calculated using an eroding algorithm with ring thickness of 5 μm.

Interstitial Distributions of Liposomes and their Contents in Spheroids

Liposomes labeled with rhodamine lipid (ex:550 nm, em:590 nm) were also passively loaded with 200 μM in PBS of the (fluid) membrane permeant CFDA SE (ex:497 nm, em:517 nm). Unentrapped CFDA SE was removed through a Sephadex G50 column, eluted in PBS at pH 7.4. Average content (CFDA SE) to lipid ratios (mg:mg) of pH-releasing and non-pH-releasing liposomes were 0.0106 ± 0.0035 and 0.0397 ± 0.0137, respectively (n = 5).

Spheroids of ~ 300 μm-in-diameter were incubated with liposomes (or the free CFDA SE) at a final concentration of 1mM lipid and 5 nM CFDA SE. After 6 hours of

incubation, spheroids were removed in a volume of 2 µL and were added to Cryochrome™ followed by overnight freezing at -80°C. Then, frozen spheroids were sliced at 20 µm thickness using a Cryotome E (Thermo Fisher Scientific, Waltham, MA). Fluorescence transmission images of slices were obtained using an Olympus IX81 fluorescence microscope with a 20x air objective. The radial distributions of liposomes and/or their contents were analyzed using an eroding algorithm with ring thickness of 5 µm. Concentrations of fluorophores were calibrated using images of solutions of known concentrations in a quartz cuvette of 20 µm path length.

Spheroid Growth and Outgrowth Assays

Once spheroids reached the appropriate size of ~ 300 µm-in-diameter they were transferred in poly-HEMA U-shaped 96-well plates and were incubated with both types of liposomal cisplatin, with not loaded liposomes and with the free cisplatin for 6 hours in a total volume of 200 µL, followed by one wash in fresh media. The 6 hour incubation was chosen to agree with the minimum expected blood circulation time of liposomes. Spheroids were then deposited onto new wells in fresh media and their growth was tracked by imaging on a daily basis until the spheroids that received no treatment reached a no growth phase.

At this point an outgrowth assay was performed. Briefly, spheroids were washed and plated on 96-flat well cell culture treated plates. The spheroids were allowed to adhere and were left to propagate until the cells from spheroids that received no treatment reached 90-100% confluency. Cells were then trypsinized and were diluted in PBS, and were counted using a Coulter Counter® Cell and Particle Counter (Z1 single threshold model) (Beckman Coulter Inc, Brea, CA). Results were normalized to the measured cell

population from spheroids that received no treatment to obtain a Percent Spheroid Outgrowth value.

Statistical analysis

Results are reported as the arithmetic mean of n independent measurements ± the standard deviation. Student's t-test was used to calculate significant differences in killing efficacy between the various constructs. *p*-values less than 0.05 were considered to be significant.

2.3: Results

Liposome characterization and content retention

Table 2.1 shows the liposome size which was similar for both lipid compositions (*p*-value > 0.05). The Zeta potential of liposomes exhibited a trend towards less negative values with lowering the pH, however the differences were not statistically significant. In general, the pH-responsive liposomes' size (115 nm) and zeta potential (-6.5 mV at physiological pH) that we obtained were comparable to values reported for the FDA approved Doxil (108 nm, -13.3 mV) and the cisplatin-containing PEGylated liposomes SPI-77 (116 nm, -9.8 mV) [32]. Loading efficiencies and drug-to-lipid ratios were comparable for pH-releasing and non-pH-releasing liposomes.

Table 2.1: Liposome Size, Zeta Potential, Loading Efficiencies of Cisplatin and Cisplatin-to-Lipid Ratios (D/L Ratios) for pH-Releasing and Non-pH-Releasing Liposomes[a]

Size (nm) (PDI) n=6	Zeta Potential pH 7.4 (mV) n=8	Zeta Potential pH 6.5 (mV) n=8	Zeta Potential pH 6.0 (mV) n=8	% Loading Efficiency n=9	D:L Ratio (w/w) n=9
pH-releasing liposomes					
115.0 ± 7.0 (0.075 ± 0.047)	-6.5 ± 2.7	-5.5 ± 2.5	-5.0 ± 2.3	2.87 ± 0.86	0.056 ± 0.022
non-pH-releasing liposomes					
123.1 ± 11.4 (0.111 ± 0.048)	-5.9 ± 2.8	-5.1 ± 2.5	-4.6 ± 1.9	3.71 ± 0.96	0.067 ± 0.025

[a] Errors correspond to standard deviations of *n* independent measurements.

In cell conditioned media, after twenty four hours of incubation, pH-releasing liposomes exhibited pH-dependent release of encapsulated cisplatin (black bars, Figures 2.1A and 2.2A). At same conditions, the retention of encapsulated cisplatin by non-pH-releasing liposomes (gray bars) was higher, and was not pH-dependent. The same trends were observed following six hours of incubation in cell conditioned media (Figures A.4A and A.5A).

Studies on cell monolayers

The amounts of cell associated cisplatin (picograms cisplatin per cell) - when compared at same extracellular concentrations of cisplatin - increased with lowering the extracellular pH from 7.4 to 6.0 only for the case of cisplatin delivered by pH-releasing liposomes (Figures 2.1B and 2.2B, and Figures A.4B and A.5B following six hour incubation). For non-pH-releasing liposomes – at same extracellular concentrations of cisplatin -, the amount of cell associated cisplatin increased mostly with increase in incubation time (Figures 2.1C and 2.2C, and Figures A.4C and A.5C following six hour incubation). Free cisplatin cell uptake was independent of the extracellular pH (Figure A.6 in the Appendix).

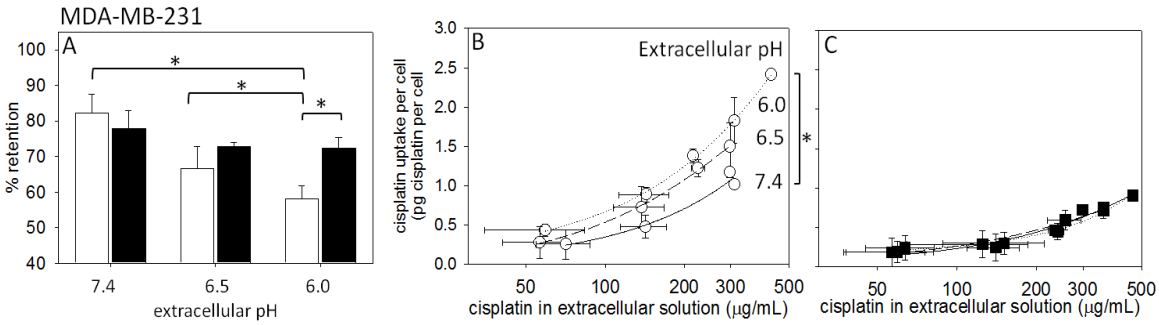

Figure 2.1: (A) Retention of encapsulated cisplatin by pH-releasing liposomes (black bars) and non-pH-releasing liposomes (gray bars) following 24 hours of incubation with MDA-MB-231 cells. Error bars correspond to standard deviations of repeated measurements. Three independent liposome preparations per data point. * indicates p-values < 0.05. (B) and (C): Uptake of cisplatin (pg of cisplatin per cell) by MDA-MB-231 cells delivered by pH-releasing liposomes (B) and by non-pH-releasing liposomes (C) following 24 hours of incubation at extracellular pH values of 7.4, 6.5, and 6.0. Black circles: pH-releasing liposomes loaded with cisplatin; gray circles: non-pH-releasing liposomes loaded with cisplatin. Error bars correspond to standard deviations of repeated measurements. Three independent liposome preparations, 2 samples per preparation. * indicates p-values < 0.05.

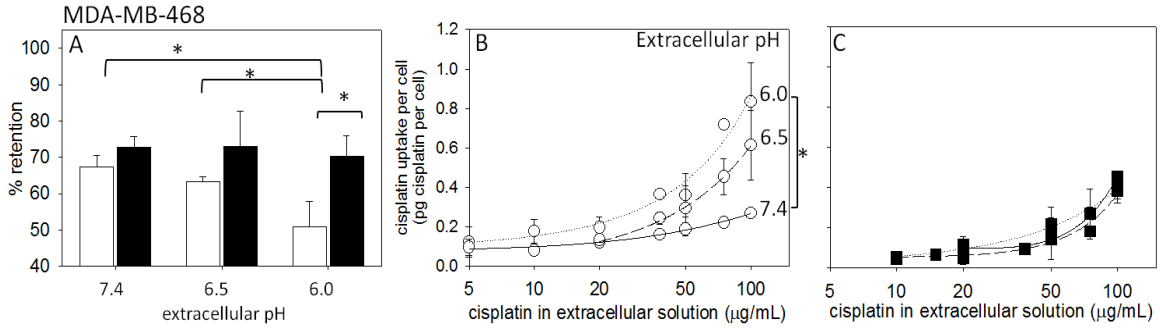

Figure 2.2: (A): Retention of encapsulated cisplatin by pH-releasing liposomes (black bars) and non-pH-releasing liposomes (gray bars) following 24 hours of incubation with MDA-MB-468 cells. Error bars correspond to standard deviations of repeated measurements. Three independent liposome preparations per data point. * indicates p-values < 0.05. (B) and (C): Uptake of cisplatin (pg of cisplatin per cell) by MDA-MB-468 cells delivered by pH-releasing liposomes (B) and by non-pH-releasing liposomes (C) following 24 hours of incubation at extracellular pH values of 7.4, 6.5, and 6.0. Black circles: pH-releasing liposomes loaded with cisplatin; gray circles: non-pH-releasing liposomes loaded with cisplatin. Error bars correspond to standard deviations of repeated measurements. Three independent liposome preparations, 2 samples per preparation. * indicates p-values < 0.05.

Liposome cell uptake was low and ranged from 0.04 to 0.10% of the total introduced liposomes, both for pH-releasing and for non-pH-releasing liposomes (see Figure A.7 in the Appendix). Accordingly, the amount of cisplatin delivered to cells by

these cell-associated pH-releasing liposomes (assuming no loss of cisplatin from liposomes before their cell uptake) was significantly less that the measured values of drug-per-cell that are reported on Figures 2.1B and 2B. In particular, in Figure 2.1B (Figure 2.2B) for cisplatin concentrations in the incubating solution above 100 μg/mL (50 μg/mL) at the acidic extracellular pH of 6.0, less than ~10% of the reported cisplatin-per-cell could be originated in pH-releasing liposomes taken up by cells and at least ~ 90% of reported cisplatin-per-cell should be originated in cisplatin which was released from pH-responsive liposomes residing in the acidic extracellular space.

On cell monolayers, only the LD_{50} values of pH-releasing liposomal cisplatin exhibited a decreasing trend with lowering pH from 7.4 to 6.0 (Table 2.2, Figures A.8 and A.9). At the lowest value of extracellular pH studied, pH 6.0, the LD_{50} values of the pH-releasing liposomal cisplatin was on average half (or less) the LD_{50} values of the non-pH-releasing liposomal cisplatin (p-values < 0.05). At neutral pH, the LD_{50} values of both liposome types were not statistically different (p-values > 0.05). The LD_{50} values of the free cisplatin were independent of pH, and were on average approximately ten times less than the corresponding IC_{50} values of the pH-releasing liposomal cisplatin (Figure A.10). Both liposome compositions not containing cisplatin decreased cell viability only at the two highest lipid concentrations used and only following the 24-hour incubation period (black squares and circles in Figures A.8 and A.9).

Table 2.2: IC_{50} values (µg/mL) of liposomal and free cisplatin as a function of pH and incubation times. Error bars correspond to standard deviations of the LD_{50} values of repeated measurements. Three independent measurements per data point. * Equal to or less than 50 % cell viability was not reached within the range of drug-to-lipid ratios which were feasible in this study.

	IC_{50} Values (µg/mL)		
	pH 7.4	**pH 6.5**	**pH 6.0**
MDA-MB-231 Cells	**6 Hours**		
pH-releasing	*	*	244.54 ± 37.51
non-pH-releasing	*	*	*
free cisplatin	40.35 ± 5.91	36.40 ± 11.43	27.44 ± 13.13
	24 Hours		
pH-releasing	*	177.76 ± 50.73	101.87 ± 24.06
non-pH-releasing	*	*	374.16 ± 20.02
free cisplatin	10.97 ± 1.94	10.50 ± 2.18	8.87 ± 3.84
MDA-MB-468 Cells	**6 Hours**		
pH-releasing	54.58 ± 19.20	55.55 ± 17.67	33.31 ± 6.89
non-pH-releasing	80.49 ± 13.20	85.63 ± 5.13	69.97 ± 14.73
free cisplatin	5.32 ± 3.99	5.37 ± 1.76	3.84 ± 2.55
	24 Hours		
pH-releasing	23.20 ± 8.04	18.22 ± 6.95	14.53 ± 3.61
non-pH-releasing	49.54 ± 19.30	50.64 ± 18.31	33.69 ± 4.96
free cisplatin	1.43 ± 0.49	4.50 ± 4.45	1.71 ± 1.42

Studies on multicellular spheroids

Spheroids formed by the MDA-MB-231 cancer cells (Figure A.11A) and by the MDA-MB-468 cancer cells (Figure A.11B) developed interstitial pH gradients with decreasing pH that reached the lower value of 6.5 ± 0.1 at the spheroid center.

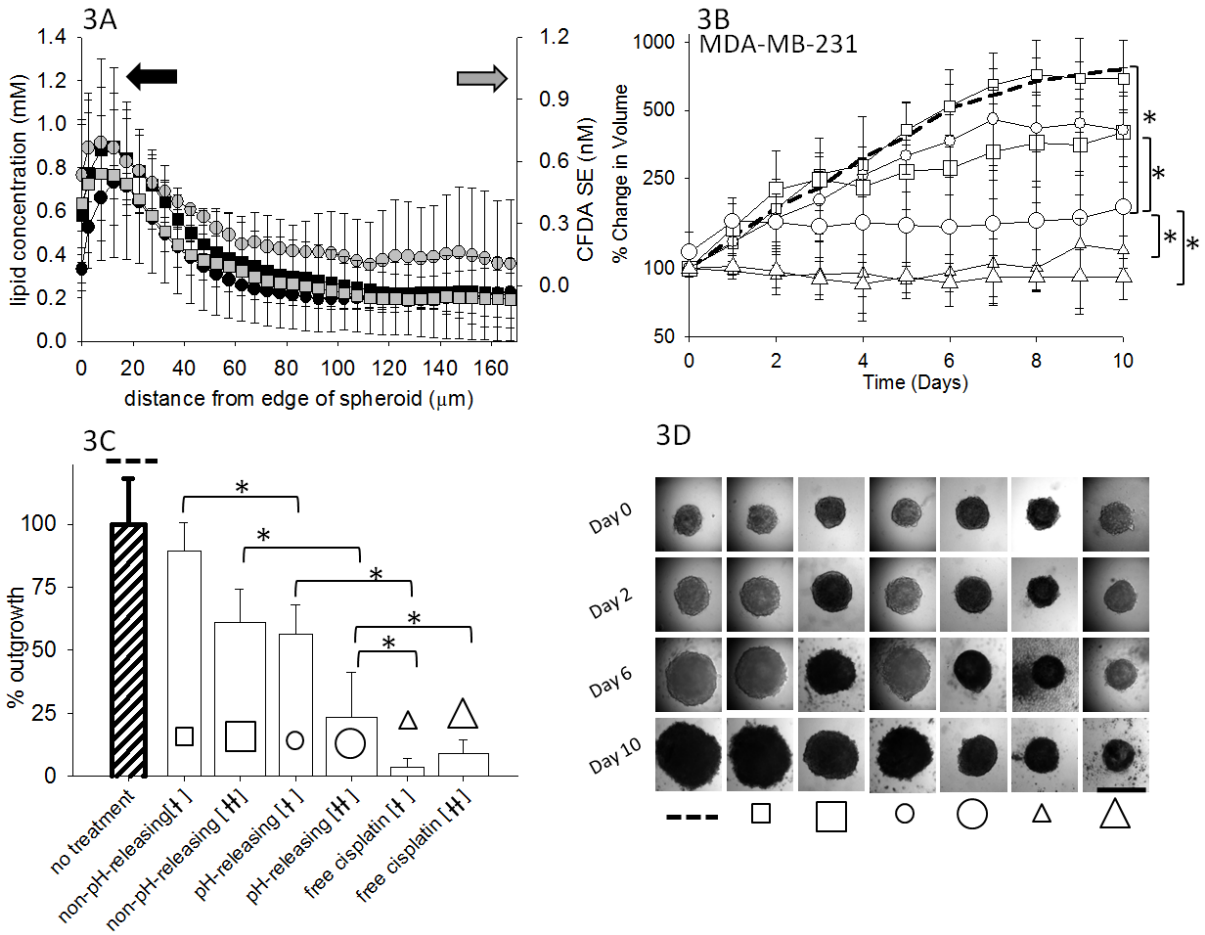

Figure 2.3: (A) Distributions of pH-releasing and non-pH-releasing liposomes (left axis) and of their contents (right axis) in multicellular spheroids of MDA-MB-231 TNBC cells. Black (gray) circles: pH-releasing (non-pH-releasing) liposomes; black (gray) squares: CFDA SE delivered by pH-releasing (non-pH-releasing) liposomes. Distributions averaged over n = 5 spheroids per case. (B) Control of MDA-MB-231 spheroid growth over time, (C) extent of outgrowth of spheroids following the end time point shown in (B), and (D) characteristic images of spheroids during monitoring of growth. Black circles: pH-releasing liposomes loaded with cisplatin; gray circles: non-pH-releasing liposomes loaded with cisplatin; white circles: free cisplatin; dashed line: no treatment. Small or ŧ (large or ŧŧ) symbols correspond to 30 μg/ml (90 μg/ml) cisplatin. Error bars correspond to standard deviations of repeated measurements. Two independent liposome preparations, 7 spheroids per treatment type per preparation. * indicates p-values < 0.05. % change in volume = V_t/V_o x 100%, where V_t is volume at time t and V_o volume before initiation of treatment. At t = 0 the average volume of spheroids was 300 ± 50 μm (n = 14 spheroids). Scale bar corresponds to 400 μm.

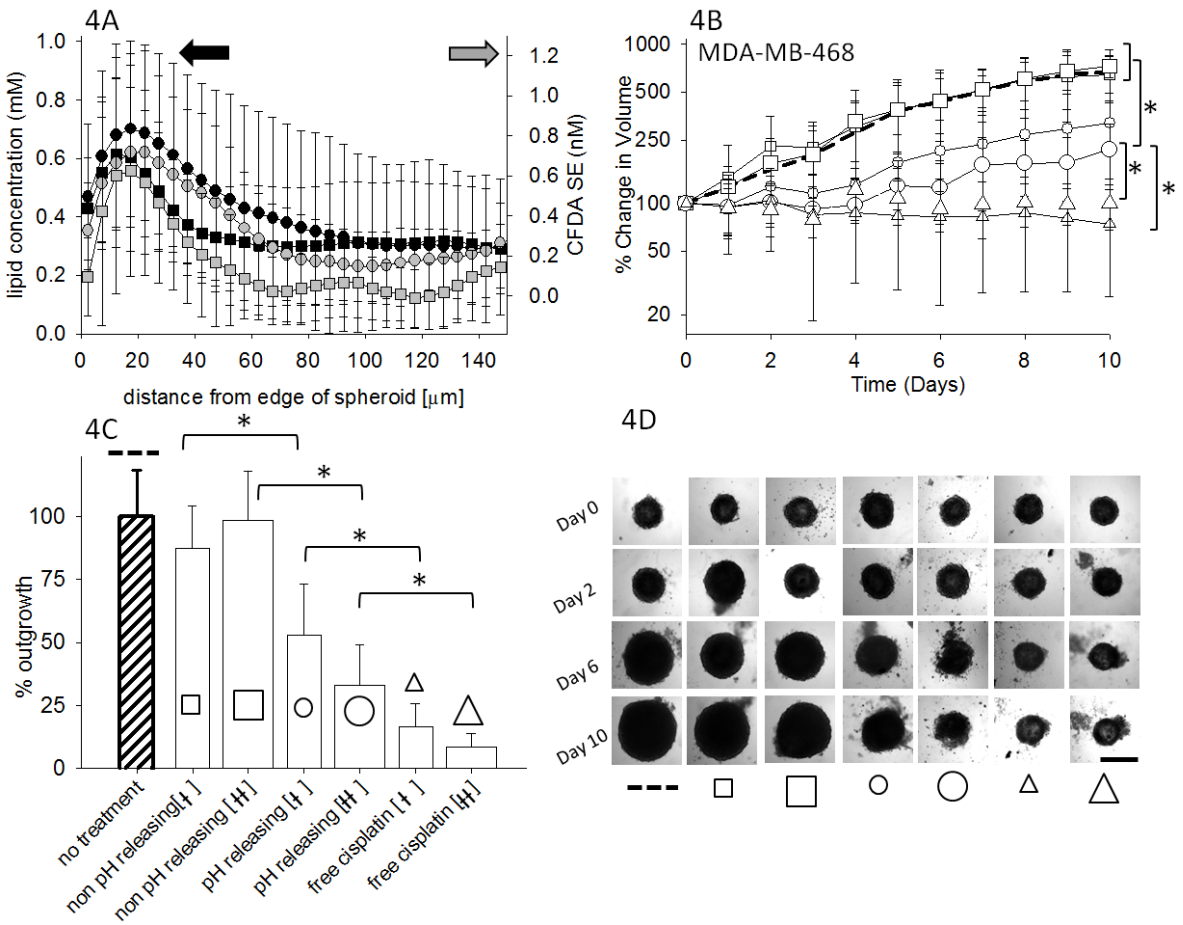

Figure 2.4: (A) Distributions of pH-releasing and non-pH-releasing liposomes (left axis) and of their contents (right axis) in multicellular spheroids of MDA-MB-468 TNBC cells. Black (gray) circles: pH-releasing (non-pH-releasing) liposomes; black (gray) squares: CFDA SE delivered by pH-releasing (non-pH-releasing) liposomes. Distributions averaged over n = 5 spheroids per case. (B) Control of MDA-MB-468 spheroid growth over time, (C) extent of outgrowth of spheroids following the end time point shown in (B), and (D) characteristic images of spheroids during monitoring of growth. Black circles: pH-releasing liposomes loaded with cisplatin; gray circles: non-pH-releasing liposomes loaded with cisplatin; white circles: free cisplatin; dashed line: no treatment. Small or ϟ (large or ǂ) symbols correspond to 15 μg/ml (45 μg/ml) cisplatin. Error bars correspond to standard deviations of repeated measurements. Two independent liposome preparations, 7 spheroids per treatment type per preparation. * indicates p-values < 0.05. % change in volume = V_t/V_o x 100%, where V_t is volume at time t and V_o volume before initiation of treatment. At t = 0 the average volume of spheroids was 300 ± 40 μm (n = 14 spheroids). Scale bar corresponds to 400 μm.

The interstitial distributions of both liposome compositions (black and gray circles) were comparable towards the center of both types of spheroids (Figures 2.3A and

2.4A; characteristic spheroid images are shown in Figure A.12). Surprisingly, on MDA-MB-468 spheroids only, although both types of liposomes had comparable size, extent of PEGylation and zeta potential, the two liposome types exhibited different profiles in the spheroid region between the edge of the spheroids and up to ~ 90 μm from the spheroids' edge. In each spheroid type, the contents delivered by the pH-releasing liposomes (black squares) showed greater penetration within the spheroid relative to the contents delivered by the non-pH-releasing liposomes (gray squares, Figures 2.3A and 2.4A).

In agreement with the interstitial distribution studies, in MDA-MB-231 spheroids, following a 6-hour incubation with 30 μg/mL (small symbols) and 90 μg/mL cisplatin (large symbols) (in media at physiologic pH), pH-releasing liposomal cisplatin (black circles) resulted in significantly smaller spheroid volumes at day 10 post treatment relative to the non-pH-releasing liposomal cisplatin (gray circles) and to no treatment (dashed line), respectively (p-values < 0.001) (Figures 2.3B and 2.3D). Correspondingly, spheroids treated with pH-releasing liposomal cisplatin exhibited only 62.9 ± 14.6 % (38.3 ± 31.1 % at the high cisplatin concentration) of the outgrowth observed for spheroids treated with the non-pH-releasing liposomal cisplatin (p-values < 0.001) (Figure 2.3C). At both cisplatin concentrations during incubation, the free form of cisplatin (white circles) outperformed both liposomal constructs, with the advantage relative to pH-releasing liposomes becoming less pronounced with increasing concentrations of cisplatin.

Similarly, in MDA-MB-468 spheroids, at 15 μg/mL cisplatin (small symbols) and at 45 μg/mL (large symbols) pH-releasing liposomal cisplatin (black circles) resulted in significantly smaller spheroid volumes at day 10 post treatment relative to the non-pH-

releasing liposomal cisplatin (gray circles) and to no treatment (dashed line), respectively (p-values < 0.001) (Figures 2.4B and 2.4D). The outgrowth assay of spheroids treated with pH-releasing liposomal cisplatin demonstrated 58.8 ± 25.5 % (33.7 ± 17.6 % at the higher cisplatin concentration) less outgrowth relative to the non-pH-releasing liposomal cisplatin (p-values < 0.001 for the incubation conditions at 15 µg/mL cisplatin) (Figure 2.4C). As with the other cell line, at both concentrations of cisplatin, free cisplatin (white circles) outperformed the liposomal forms of cisplatin, with the advantage relative to pH-releasing liposomes becoming less pronounced at the higher concentration of cisplatin. In both spheroid types, pH-releasing and non-pH-releasing liposomes which were not loaded with cisplatin did not affect growth (Figure A.13 and Figure A.14).

2.4: Discussion

In this study, multicellular spheroids were used as surrogates of the tumors' avascular regions, and the role of interstitial distributions of cisplatin on affecting its efficacy to control the growth of spheroids was evaluated. Limited drug penetration and heterogeneous drug distributions within tumors [6, 24] have been largely associated with the observed limited efficacy of chemotherapeutics *in vivo* contrary to their efficacy *in vitro* on cell monolayers, in the absence of diffusion-limited transport. Multicellular spheroids have been suggested in various contexts as reasonable *in vitro* surrogates capturing the above conditions [33] The effects on tumor penetration of particle surface characteristics and size have been studied *in vivo* [34].

In our study, delivery of cisplatin by pH-releasing liposomes, which are activated to release cisplatin in the spheroids' acidic interstitium (7.0 < pH < 6.4 or 6.0 in some

human cancers [19, 20]), resulted in better control of spheroids' growth relative to delivery of cisplatin by liposomes without the pH-releasing property. The studies on multicellular spheroids indicated a strong correlation between better control of spheroid growth and lower extents of spheroid outgrowth with deeper penetration within the spheroid of the contents of liposomes. In these studies, both pH-releasing and non-releasing liposomes exhibited similar limited penetration at the spheroids' core region.

Molecular modifications of cisplatin (carboplatin, oxaliplatin and others) [11] have been previously explored to address its limited water solubility and toxicity, usually resulting in improved therapeutic index attributed mostly to lower organ toxicities than to greater activities [35, 36] . Several liposomal approaches of cisplatin - to address toxicities by modification of the drug biodistributions - have been extensively investigated in reported literature [5, 13] and include targeted approaches [37] heat activated delivery approaches [29] and most notably Lipoplatin^{TM} which was shown to exhibit enhanced or similar efficacy to cisplatin, as monotherapy, in a phase III study pH-responsive release of cisplatin from liposomes has also been reported, but involves activation at pH values (at pH ~ 5.5) associated with the endosomal compartment following liposome internalization by cells [5]. We have previously reported the significance of the interstitial release of a different chemotherapeutic, doxorubicin, to address its heterogeneous distributions in multicellular spheroids used as analogues of the tumors' avascular region [38]. Doxorubicin's plasma membrane permeability, however, is affected by the slightly acidic interstitial pH decreasing, therefore, its efficacy. This is not the case for cisplatin as demonstrated in this study (Figure A.4).

Cisplatin is, to a great extent, a cell membrane-permeant agent (not affected by the extracellular pH in the range of values related to the tumor interstitium) that exerts its anticancer effect mainly by its intercalation to the nuclear DNA [11] The findings on Figure 2.5 demonstrated that viability of cells (in monolayers, i.e. in the absence of diffusion-limited transport) was a strong function of the DNA-cisplatin adducts independent of the delivery modality of cisplatin or of the extracellular pH. Therefore, these findings suggest that increased extracellular concentrations of free cisplatin in the vicinity of cancer cells, mediated by pH-releasing liposomes for example, may be used as a potential delivery approach to enhance efficacy while decreasing nephrotoxicity, neurotoxicity, ototoxicity and gastrointestinal toxicities caused by administration of cisplatin in free form [11].

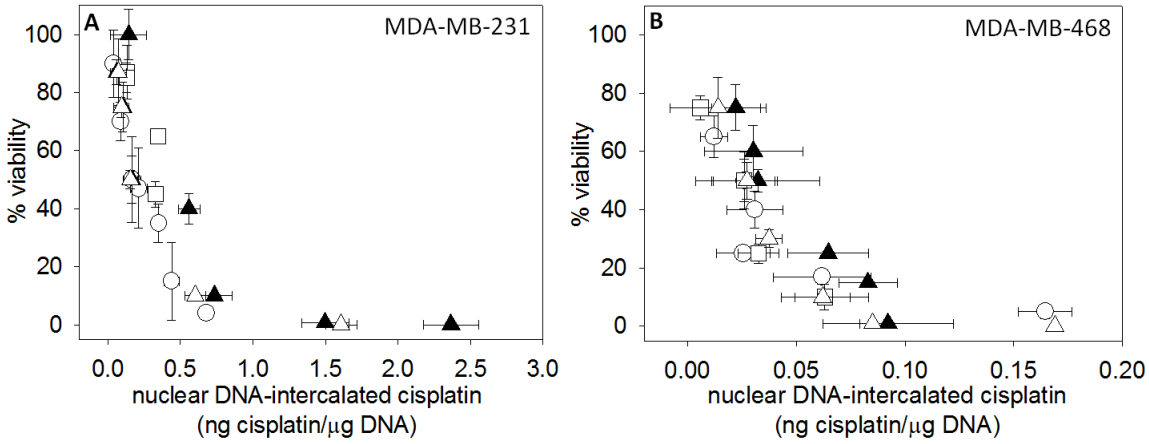

Figure 2.5: Viability of MDA-MB-231 (A) and MDA-MB-468 (B) as a function of nuclear DNA-associated cisplatin for pH-releasing (black circles) and non-pH-releasing (gray circles) liposomal cisplatin and free cisplatin (white circles) at different extracellular pH values. Black circles: pH-releasing liposomes at extracellular pH 6.0; gray circles: non-pH-releasing liposomes at extracellular pH = 6.0, white circles with cross: free cisplatin at extracellular pH 6.0; white circles: free cisplatin at extracellular pH 7.4. Error bars correspond to standard deviations of repeated measurements. Three independent preparations of liposomes; 1-2 samples per preparation.

The efficacy of free cisplatin relative to pH-releasing (and non-pH-releasing) liposomal cisplatin is undoubtedly better both in the absence and in the presence of diffusion-limited transport (on cell monolayers and on multicellular spheroids, respectively). However, reported values of MTDs for these different forms of cisplatin are different. In particular, in humans following i.v. administration, the MTD for free cisplatin (100-120 mg/m^2 with standard hydration [39]) is reported to be almost three times lower than the MTD for (non-pH-releasing) liposomal cisplatin (300 mg/m^2 [40]). In this context, and given that pH-releasing liposomes are expected to have similar pharmacokinetics to those of non-pH-releasing liposomes [41], comparison in our studies of free cisplatin to the pH-releasing liposomal cisplatin at three times greater the concentration of cisplatin, may be justifiable. At these conditions, in terms of spheroid growth/outgrowth control, the not so different efficacies for the two forms of cisplatin (small white circles for free cisplatin and large black circles for 3-fold pH-responsive liposomal cisplatin in Figures 3B, 3C and 4B, 4C) were suggestive of the potential for improved therapeutic index by the pH-releasing liposomal approach. *In vivo* additional factors including blood clearance and potential liver toxicities caused by liposomal delivery, and possibly other factors, may affect the therapeutic index of pH-releasing liposomes, and these studies are currently under investigation.

Although the focus of this study is not to address the multivariable resistance mechanisms of cisplatin, [42, 43] its transport-related resistance mechanisms could in principle be affected. Given that the efflux and influx of cisplatin (that is collectively attributed to membrane transporters and to passive transmembrane diffusion [43]) are dependent on its extracellular concentration [44] and exposure time [44, 45], it could be

possible that by increasing - with pH-releasing liposomes - the amount and residence time of free cisplatin in the extracellular space of cancer cells, within the tumor interstitium, to partly bypass the platinum resistance of cells.

CHAPTER 3: GROWTH RATE DISSIPATION OF METASTATIC TRIPLE NEGATIVE BREAST CANCER ATTRIBUTED TO SLOW TUMOR-CLEARING AND DEEP TUMOR-PENETRATING CHEMOTHERAPY

Note: data in this chapter was adapted from the following manuscript which is in preparation:

Stras, S.; Sofou, S "Growth rate dissipation of metastatic triple negative breast cancer attributed to slow tumor-clearing and deep tumor-penetrating chemotherapy" In Preparation.

3.1: Introduction

Triple Negative Breast Cancer (TNBC) accounts for 10-20% of breast carcinomas with the lowest 5-year survival rates among all breast cancer patients [46]. TNBC is defined as being negative in gene expression for the estrogen, progesterone, and HER2/neu receptors, and encompasses a particularly heterogeneous group of tumors [46]. Currently, metastatic TNBC is incurable.

In general, platinum-derived agents [47] receive extensive clinical use because of their DNA damaging activity to which TNBC tumors frequently show sensitivity [3], [48]. However, the poor prognosis [3, 7] in metastatic TNBC is attributed partly to the lack of *targeted therapies* (receptor-mediated therapies, [49] and/or tumor-mediated therapies [49]) and largely to the lack of therapeutic modalities that *effectively deliver* doses at *lethal levels* at the sites of disease. Clinical results on experimental receptor-mediated targeted therapies to patients with TNBC designed to affect or inhibit key signaling

pathways [50, 51] did not demonstrate statistically significant improvement following single-agent targeting approaches or in combination with platinum agents [52]. Of lower toxicities but not yet determined improvement in therapeutic effect were also the clinical results of liposomal cisplatin (CDDP) which was designed as a tumor-mediated targeting modality utilizing the EPR effect [13, 53].

The efficacy of tumor delivered doses can be enhanced when delivered by carriers which improve the uniformity in intratumoral drug distributions [54]. We have previously demonstrated *in* 3D multicellular spheroids (used as surrogates of the tumor avascular regions) that this goal can be facilitated by nanocarriers engineered to release their (rapidly diffusing) therapeutic contents in the tumor interstitium enabling deep tumor-penetration of therapeutics [55, 56]. Key to this approach is to use drug nanocarriers that do not become internalized by cells - so as to maximize the fraction of released drug that may penetrate deeper in the tumor - and, to choose therapeutic agents (for example, cisplatin) which are efficiently transported across the cell membranes independent of the local extracellular milieu.

However, to effectively translate this strategy *in vivo*, the intratumoral residence times of such drug-loaded nanocarriers should be increased to maximize the time-integrated dose delivered at the tumor. In this study, to increase the nanocarriers' tumor residence times, we introduce an 'adsorptive/adhesive switch' on the nanocarriers' surface with the aim to slow down their tumor-clearing kinetics. The switch is designed to promote nanoparticle adsorption on cancer cells and/or the ECM while keeping their internalization by cells to a minimum.

Herein, we present lipid-based nanocarriers (liposomes) loaded with cisplatin and designed to combine the above two distinct mechanisms (of improving intratumoral drug uniformity and maximizing the carriers' tumor residence times) with the goal of enabling better growth control of TNBC metastases *in vivo*. Both mechanisms were chosen to be activated in the slightly acidic pH of the tumor interstitium (pH ~ 6.7 - 6.0) [57, 58].

In particular, first, for tumor interstitial release, liposomes were designed to contain pH-responsive lipid membranes forming reversible phase-separated lipid domains (resembling lipid patches) with lowering pH as we reported before [59-62]. During circulation in the blood, these liposomes comprise well-mixed, uniform membranes and stably retain their encapsulated contents. In the acidic tumor interstitium, occurrence of lipid-phase separation results in formation of lipid patches that span both lipid leaflets (patch cross-bilayer registration) [63]. We have demonstrated that this lipid rearrangement in the bilayer membrane can be utilized to create pronounced grain boundaries around the lipid patches enabling release of the encapsulated therapeutic agents which then - in a drug delivery setting - may diffuse deeper into solid tumors [55, 56]. At the molecular level, lipid phase separation is enabled by balancing the permanent hydrogen-bonding attraction with the pH-tunable electrostatic repulsion between the lipids that form the domains (lipids with phosphatidyl serine headgroups, in this study). The extent of membrane permeability on phase-separated bilayers was previously shown to be affected by the order of transient defects in the packing of lipid acyl-tails along the domain boundaries. Packing discontinuities along these boundaries may be enhanced by incorporation of saturated, gel-phase lipids with acyl-tails of different lengths [61].

Second, the adsorptive switch - which is an electrostatic switch - attributing positive charge on the liposome corona - and, therefore, increasing the liposomes' tendency to adsorb on cells and the ECM [64, 65]- was introduced by the chemical moiety dimethyl ammonium propane (DAP). DAP was conjugated on the free end of PEG which is used in the form of PEGylated lipids (Figure 1, the molecule's structure). The intrinsic pKa of the free DAP is approximately 6.7 [66] comparable to the pH values in the tumor acidic interstitium. The design of this switch is based on the rationale that during liposome circulation the PEGylated corona of the nanocarrier would not be positive, and , therefore, liposomes would exhibit low tendency to adsorb on anionic surfaces. Upon tumor internalization and liposome diffusion towards the tumor acidic interstitium, protonation of the DAP-PEG-lipids would attribute a cationic charge on the liposome PEGylated corona potentially increasing their adsorption to anionic surfaces, namely the cells and the ECM. Contrary to previously reported DAP-containing liposomes and other particles, the titratable charge was designed to be located at the edge of the PEG corona and not conjugated on the lipid headgroups. This surface architecture was hypothesized and was demonstrated, in this study, to minimize the internalization of these liposomes by cells, and to essentially delay their clearance from the tumor because of their electrostatic adsorption on extracellular compartments within the tumor and not because of their internalization by cells.

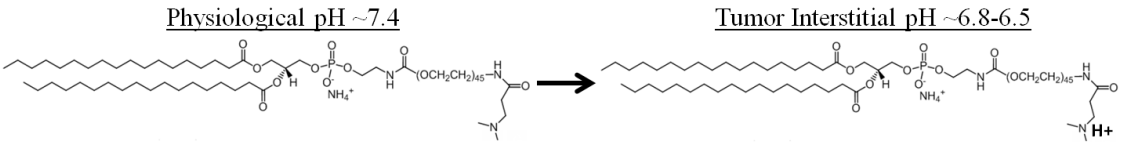

Figure 3.1: Structure of 18:0 PE- PEG_{2000}- DAP (dimenthylammonium propanoyl). Custom synthesized from Avanti Polar Lipids. DAP group becomes positively charged with acidic pH (pKa ~6.7).

In this study, we characterize the extent of pH-responsive drug release from liposomes and the pH-responsive change in the charge of DAP-functionalized liposomes resulting in their slower clearance from spheroids as a demonstration of cell/ECM increased adsorption. We evaluate the significance of each property in 3D multicellular spheroids of TNBC cells and of cells derived from TNBC metastases. We also demonstrate the effect of each of these properties and of their combination in liposomal chemotherapy on controlling the growth of TNBC metastases, and we correlate these findings to the drug residence times in tumors mediated by each of these constructs.

3.2: Materials and Methods

Materials

All lipid products were obtained from Avanti Polar lipids (Alabaster, USA) including 1,2-distearoyl-sn-glycero-3-phosphocoline (DSPC), 2-diheneisocanoyl-sn-glycero-3-phosphocoline (21PC), 1,2-dioctadecanoyl-*sn*-glycero-3-phospho-L-serine (sodium salt) (DSPS), 1,2-distearoyl-sn-glycero-3-phosphoethanolamine-N-[amino(polyethylene glycol)-2000](ammonium salt) (DSPE-PEG), and 1,2-dipalmitoyl-sn-glycero-3-phosphoethanolamine-N-(Lissamine Rhodamine B Sulfonyl) (Ammonium

Salt) (DPPE-Rhodamine). The functionalized lipid 1,2-distearoyl-sn-glycero-3-phosphoethanolamine-N - PEG_{2000}-dimenthylammonium propanoyl (DSPE-PEG-DAP) was custom synthesized by Avanti Polar lipids. Cholesterol , cis-diamminedichloroplatinum (II) (CDDP), phosphate buffered saline (PBS) tablets, Sephodex G-50 resin, Sepharose 4B resin, and chloroform were purchased from Sigma – Aldrich Chemical (Atlanta, GA). Polycarbonate membranes (100 nm pore size) for extrusion, and extruder setups were purchased from Avestin (Ottawa, ON, Canada). Ethylenediamine Tetraacetic Acid, Disodium Salt Dihydrate (EDTA) and SNARF-4F were purchased from Thermo Fisher Scientific (Waltham, MA). Filters used for sterilization, with 200 micron pore diameters, were purchased from VWR (Radnor, PA).

Cell Lines

MDA-MB-231 and MDA-MB-436 human breast cancer cell lines were obtained from the American Type Culture Collection (ATCC, Rockville, MC, USA). MDA-MB-231 cells were cultured in DMEM Media, MDA-MB-436 cells were cultured in RPMI 1640, both supplemented with 10% fetal bovine serum and 1% penicillin streptomycin 100x solution at 37°C with 5% CO_2 and 95% air. Mice sublines were developed in house by removing the primary and metastatic tumors present in NSG female mice, by grinding them and plating them in petri dishes with DMEM media. Cells were grown in an incubator at 37°C with 5% CO_2 and 95% air. After several weeks only MDA-MB-231 subline cells remained which were propagated and stored in liquid nitrogen vapor phase, and, when needed, were thawed in DMEM media. Media was purchased from ATCC, fetal bovine serum was purchased from Omega Scientific (Tarzana, CA) and penicillin streptomycin was purchased from Fisher Scientific (Waltham, MA). Matrigel^{TM} used in

the formation of multicellular spheroids was also purchased from Fisher Scientific. Before incubation with cells, all liposomes were sterilized with 200 micron filters purchased from VWR (Radnor, PA).

Liposome Preparation and Loading of Cisplatin

The liposome compositions studied herein include a pH-releasing and a non-pH-releasing structure containing 21PC:DPPS:Cholesterol:DSPE-PEG at 0.51:0.33:0.08:0.08 mole ratios and DSPC:DSPS:Cholesterol:DSPE-PEG at 0.56:0.24:0.12:0.08 mole ratios, respectively, as reported before [67]. Both liposome types were functionalized with 8-10 mole % DSPE-PEG-DAP replacing the non-functionalized DSPE-PEG lipid. All compositions were labeled with 0.125 mole % DPPE-Rhodamine lipid. Liposomes were prepared using the thin film hydration method (ref: sally Mol Pharm). Briefly, the dry lipid film (10 to 80 μmoles total lipid) was hydrated with 1 mL of PBS (10 mM phosphate buffered saline with 1 mM EDTA) at pH 7.4, and this suspension was then annealed at 60°C for 2 hours following extrusion through two stacked 100 nm sized polycarbonate membranes 21 times at 80°C. Cisplatin was then passively loaded into liposomes - which were first purified by a Sepharose 4B column from any micellar forms as previously described [55]. After loading, unencapsulated Cisplatin was removed from liposomes by size exclusion chromatography using a Sephadex G50 column, eluted with PBS at pH 7.4. An aliquot of the collected liposome fraction was lysed with 0.5% Triton-X 100, and the platinum content was measured using a Graphite Furnace Atomic Absorption Spectrophotometer (Buck Scientific, using a Hollow Cathode Pt 365.9 nm lamp) and quantified by comparison to a calibration curve as reported before [55]. The lipid content was evaluated using the Stewart's Assay [68].

Liposome Characterization

The size and zeta potential of liposomes were determined using a Zetasizer Nano ZS 90 (Malvern, United Kingdon). Samples were diluted in 1X PBS (300 mOsm) or low salt PBS (30 mOsm salt concentration), respectively. Retention of Cisplatin by liposomes was performed in 10% FBS cell culture media in the presence of cells, for a 6-hour incubation period. At the end of the incubation the liposome suspension (without cells) was run through a Sephadex G50 column to remove released Cisplatin from liposomes, and the content of platinum in the collected fractions was quantified using the GFAAS.

Cell Binding and Internalization

To quantify the percent liposomes bound to cells, liposomes labeled with 2 mole % 16:0-rhoadmine, were added to suspensions of 1 million MDA-MB-231 (ATCC) cells at a concentration of 0.25 mM in cell culture media at pH 7.4 or 6.5. After 6 hours of incubation at 4°C, cells were washed with appropriately pH'd PBS buffer and trypsinized. Cells were spun down and resuspended in 1 mL dI water and sonicated for 10 minutes. After sonication, 1 mL of acidified IPA (10% HCl, 90% IPA) was added to the samples which were then read on a spectrofluorometer using rhodamine to detect the presence of liposomes (ex. 550 nm, em. 590 nm).

Evaluation of IC50s on cell monolayers

To determine the IC50 of the liposomal Cisplatin and of the free Cisplatin, 20,000 cells per well were plated in a 96-well plate. A range of concentrations of sterilized liposomes (containing or not Cisplatin) or of free Cisplatin was added to the wells mixed in media (with 10% FBS) at pH 7.4 or pH 6.5. Upon completion of the 6 hour incubation,

cells were washed twice with PBS and fresh media, supplemented with 10% FBS, was then added to the wells. After two doubling times an MTT assay (Promega, Madison, WI) was performed (following the vendor's instructions) to determine percent cell viability. Absorbance was read at 570 nm.

Spheroid Formation and Characterization

Formation of MDA-MB-231 spheroids was described previously.[55] To form spheroids using MDA-MB-231 sublines (which were developed as mentioned above) or the MDA-MB-436 cell line, cells were trypsinized and diluted in DMEM or RPMI 1640, respectively, with 2.5% (v/v) Matrigel™. Cells were plated at a density of 150-175 cells per well in polyHEMA coated u-shaped 96-well plates. Media, plates, and materials were kept at 4°C to prevent solidification of Matrigel™. Plates were then spun at 1000 x g for 3 minutes to pellet cells, and after 10-11 days spheroids reached the desired size of 400 micrometers in diameter.

To determine the interstitial pH gradients, spheroids, at a size of 300 ± 30 μm, were incubated overnight with SNARF-4F, a membrane impermeant pH indicator (ex: 488 nm, em: 580 nm and 640 nm) whose ratio of intensities in the red and the green channels were pH dependent [55]. After a 12 hour incubation with SNARF-4F the spheroids were washed and placed in wells of fresh media for imaging using a Zeiss LSM510 Laser Scanning Confocal Microscope. Ten micrometer thick z-stacks were obtained through the entirety of the spheroid to allow identification of the equatorial optical slice on which an in-house erosion algorithm was used to calculate the average intensities in both the green and the red channel on 5 μm concentric rings from the edge

of the optical slice to the core. The fluorescent intensities of ring averaged intensities on equatorial slices of spheroids not incubated with SNARF-4F were subtracted from the above fluorescent images to correct for background noise. A calibration curve of the ratios of the SNARF-4F intensities in the red and green channels in media of different known pH values was used to correlate the spheroid radial red/green average ratios to the spheroid interstitial pH.

To determine the uptake and clearance of liposomes and their contents, liposomes were prepared with 1 mole % 16:0 rhodamine-lipid (ex 550, em 590) and loaded with CFDA-SE (ex 497 em 517); final CFDA-SE concentration was 800 nM. Average CFDA:Lipid mole ratios for all constructs were similar; 0.520 ± 0.014. The CFDA-SE loaded liposomes were incubated with spheroids to determine uptake, and after 6 hours spheroids were moved to fresh wells of media to determine the clearance. Liposomes were added to the wells at a 1 mM lipid concentration, and a 40 nM CFDA concentration. Time points were taken at 1 hour, 3 hours and 6 hours uptake. After the 6-hour incubations spheroids were moved to fresh wells to begin the clearance phase and time points were taken at 0.5, 1, 2, 4 and 24 hour clearance. At each time point the spheroids were sampled in a volume of ~ 1 µL and frozen in cryochrome gel at -80°C. Spheroids without any treatment were frozen to be used as background. The samples were then sliced on a Cryotome at 20 µm thickness and these slices were imaged on an Olympus IX80. Calibration curves were performed using the liposomes of known concentrations which were diluted appropriately and added to a quartz cuvette of 20 µm optical path length.

Images were analyzed using an in-house developed eroding code in Matlab, which takes an average intensity of each 5 μm concentric ring of the spheroid from the edge to the core. The results were integrated over time to express the time integrated Lipid or CFDA radial concentrations for each construct.

Spheroid treatment

Spheroids were incubated with treatment for 6 hours, washed once, and then moved to wells of fresh media to be tracked over the course of 11-13 days. Spheroids were imaged every day and a % change in volume (V_t/V_o x 100) was determined over the course of the experiment. Once the control spheroids (no treatment) reached a plateau in growth, the spheroids were plated on cell culture treated 96-well plates and allowed to adhere and grow. When the control spheroids reached confluency in their wells the cells were trypsizined and counted using a Z1 Coulter Counter to determine a percent outgrowth. Spheroid growth control and outgrowth experiments were performed in duplicates with a total of 14-16 spheroids per construct.

Animal studies

NSG Mice (4-5 weeks old) purchased from Johns Hopkins University Breeding Facility were inoculated with 500,000 MDA-MB-231 cells, in a volume of 100 μL of serum free media, in the 2nd mammary fat pad. Tumor growth was tracked over time and when they reached a size of 160-200 mm^3 the primary tumors were removed surgically. After approximately 2.5 weeks mice were imaged using MRI and formation of metastatic tumors was initially confirmed in the auxillary lymph node (ALN). As time went on

formation of metastatic tumors progressed to the cervical lymph nodes (CLN), brachial lymph nodes (BLN), lungs and liver.

Mice were treated with all types of liposomal cisplatin and with free cisplatin at the same injected dose of 7.5 mg/kg of cisplatin which was injected intravenously (through the retro-orbital cavity). Treatment groups consisted of 5-7 animals and injections were performed 3 times, in 5 day intervals, beginning when formation of metastatic tumors was confirmed via MRI imaging. The diameters of metastatic tumors at the start of therapy ranged from 0.25 cm to 1.0 cm, some mice having up to 2 or 3 metastatic sites. The location of metastases at the start of the experiment was limited to auxillary and several cervical lymph nodes; ALN and CLN respectively.

During the treatment phase mice were weighed every 2 days, or every day when the growth of metastases had progressed, to check for weight loss. Grounds for euthanasia consisted of $\geq$ 10% weight loss, ulceration of metastasis, or the metastatic site reaching a size larger than 20 cm x 20 cm. Mice were scanned using an MRI once a week over the course of the experiment, and on the day they were euthanized to determine the endpoint. To determine change in volume of metastases over the course of the experiment images were analyzed using Vivoquant software.

Statistical Analysis

Results are reported as the arithmetic mean of n independent measurements ± the standard deviation. Student's t test was used to calculate significant differences in killing efficacy between the various constructs. *p*-values less than 0.05 were considered to be significant.

3.3: Results

The purity of DSPE-PEG-DAP lipid was >99% as reported by Avanti Polar Lipids (details on custom synthesis results in Figure A.15). The functionalized lipid, structure shown in Figure 3.1, was designed with the rationale to attribute a titratable charge on the PEG corona of liposomes as follows. DAP's pKa is reported to be 6.7 [66], so incorporation of the DSPE-PEG-DAP lipid in liposomes would enable increasingly more positive charge on the nanoparticles with lowering pH from 7.4 (while in the blood stream) to 6.5 (chosen herein to represent the average tumor interstitial pH value).

Table 3.1 shows that the zeta potentials of pH-releasing liposomes with DAP, and non-pH-releasing liposomes with DAP exhibited significantly lower Zeta potential values with lowering pH from 7.4 to 6.5 contrary to liposomes not functionalized with DAP-lipid (p-value < 0.01). Liposomes, regardless of composition, had similar sizes ranging from 109 to 121 nm. Loading efficiencies of liposomes with Cisplatin ranged from 2.9 to 4.3% and Drug-to-Lipid Ratios (D:L) (w/w) ranged from 0.048 to 0.060, which were all comparable between liposome compositions. Liposomes functionalized with DSPE-PEG-DAP exhibited significant cell adsorption with lowering pH from 7.4 to 6.5 as shown in Figure 3.2 both at 4°C.

Table 3.1: Liposome Size, PDI, Zeta Potentials, % Loading Efficiencies and Drug to Lipid (w/w) Ratios of All Liposomal Constructs[a]

Construct	Size (nm) (PDI) n = 6	Zeta Potential (mV) pH 7.4 n =5	Zeta Potential (mV) pH 6.8 n = 5	Zeta Potential (mV) pH 6.5 n = 5	% Loading Efficiency n = 5	D:L Ratio (w/w) n = 6
pH-releasing liposomes with DAP	121 ± 12 (0.073 ± 0.055)	-4.8 ± 0.8	-1.9 ± 0.9	-0.9 ± 0.9	4.0 ± 1.8	0.058 ± 0.010
pH-releasing liposomes without DAP	121 ± 9 (0.094 ± 0.033)	-5.9 ± 1.5	-5.4 ± 0.6	-6.0 ± 1.5	4.3 ± 1.9	0.060 ± 0.006
non-pH-releasing liposomes with DAP	121 ± 7 (0.093 ± 0.061)	-4.3 ± 1.3	-1.9 ± 1.7	-0.3 ± 1.7	3.1 ± 1.1	0.055 ± 0.008
non-pH-releasing liposomes without DAP	109 ± 19 (0.081 ± 0.024)	-6.3 ± 1.1	5.5 ± 1.2	-5.7 ± 1.4	2.9 ± 1.5	0.048 ± 0.007

[a] Errors correspond to standard deviations of *n* independent measurements

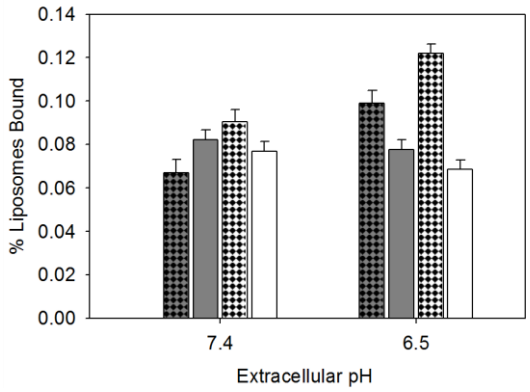

Figure 3.2: Effect of the PEGylated DAP-molecule on the extent of liposome adsorption to MDA-MB-231 (ATCC) cells at 4^0C as a function of pH. Cells were incubated at a liposome to cell ratio of $1x10^6$:1 liposomes : cell. Grey checkered bars: pH-releasing liposomes with DAP, solid grey bars: pH-releasing liposomes without DAP, solid white checkered bars: non-pH-releasing liposomes with DAP, white bars: non-pH-releasing liposomes without DAP.

Figure 3.3 shows that pH-releasing liposomes, independent of the presence or absence of DAP, exhibited a significant release (approximately 15%) of encapsulated cisplatin at pH 6.5 relative to pH 7.4 (p-values < 0.01). As expected, non-pH-releasing liposomes, again independent of the presence or absence of DAP, exhibited stable retention of encapsulated Cisplatin that was not affected by the pH acidification.

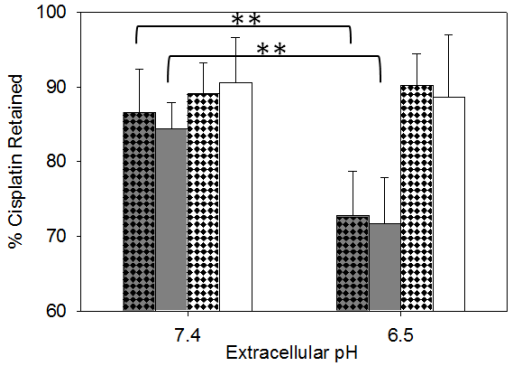

Figure 3.3: Retention of cisplatin from liposomes vs. pH following a 6-hr incubation in the presence of MDA-MB-231 (ATCC) cells. Grey checkered bars: pH-releasing liposomes with DAP, solid grey bars: pH-releasing liposomes without DAP, white checkered bars: non-pH-releasing liposomes with DAP, solid white bars: non-pH-releasing liposomes without DAP. ** indicates *p*-values < 0.01.

Evaluation of IC50 values on cell monolayers

The following cell lines were evaluated in this study: the TNBC cell lines MDA-MB-231 and MDA-MB-436 as obtained from ATCC, and three sub lines which were derived from the animal model, namely, the MDA-MB-231-PRI3 which was derived from the primary orthotopic MDA-MB-231 xenograft tumor (PRI) of mouse 3, the MDA-MB-231-ALN2 which was derived from an axillary lymph node (ALN) metastasis from mouse 2 and MDA-MB-231-LUNG1 which was derived from lung (LUNG) surface metastases of mouse 1(sub line characterization shown in Table A.1). These metastatic sites were chosen due to their frequency in appearance: ALN metastases were detected in 45 out of 45 (100%) and lung metastases we detected in 45 out of 45 mice (100%). The MDA-MB-436 is a BRCA-1 mutated TNBC cell line exhibiting aberrant DNA double-strand break repair mechanisms which to some extent have been the basis for increased clinical use of platinum-derived agents [47] against TNBC [3][48].

Table 3.2 shows that the IC50 values of the free drug (cisplatin) were independent of the extracellular pH. The cell line MDA-MB-436 was more sensitive to the platinum compound, in agreement with previous reports [69]. Interestingly, the MDA-MB-231 cell line and its animal derived sub-lines exhibited comparable drug sensitivities at a given pH so the subsequent evaluation of liposomal cisplatin forms was performed on the MDA-MB-231 (and on MDA-MB-436) as obtained from ATCC.

The killing efficacy of these liposomes is thought to be mostly based on their ability to release extracellularly their therapeutic contents - cisplatin - which then diffuse across the plasma membrane. Even DAP-functionalized liposomes did not exhibit significant extent of internalization by cells which is one of the key design points of our strategy. Table 3.2 shows that liposomes with the pH-releasing property resulted in measurable IC50 values which were higher than the corresponding IC50 values of the free drug. As expected by the design of their pH-responsive lipid membranes, these liposomes were more lethal (significantly lower IC50 values) at the more acidic extracellular pH. The presence or absence of DAP on the pH-releasing liposomes did not affect the IC50 values because even in the fully cationic form (liposomes with DAP at pH 6.5) these liposomes did not significantly become internalized by cells but, rather, they were mostly electrostatically attached on cells (Figure 3.2). The significance of this property was hypothesized to delay the tumor clearance kinetics of liposomes (*vide infra*). Table 3.2 shows that non-pH-releasing liposomes, independent of the presence or absence of DAP, did not release - extracellularly - adequate amounts of the encapsulated

Table 3.2. Free Cisplatin and Liposomal Cisplatin IC50 values. Values are the averages and standard deviations of three independent liposome or free cisplatin preparations.

	Free Cisplatin (μM)		pH-releasing Liposomes with DAP (μM)		pH-releasing Liposomes without DAP (μM)		non-pH-releasing Liposomes with DAP (μM)		non-pH-releasing Liposomes without DAP (μM)	
Cell Line	**pH 7.4**	**pH 6.5**	**pH 7.4**	**pH 6.5**	**pH 7.4**	**pH 6.5**	**pH 7.4**	**pH 6.5**	**pH 7.4**	**pH 6.5**
				**		**				
MDA-MB-436 (ATCC)	**0.74 ± 0.27**	**0.96 ± 0.22**	**129.6 ± 13.5**	**67.0 ± 19.2**	**145.4 ± 26.2**	**72.0 ± 3.4**	**undetectable**	**undetectable**	**undetectable**	**undetectable**
MDA-MB-231 (ATCC)	**45.2 ± 8.2**	**47.7 ± 4.4**	**undetectable**	**395.2 ± 58.0**	**undetectable**	**432.4 ± 33.0**	**undetectable**	**undetectable**	**undetectable**	**undetectable**
MDA-MB-231 (PRI3)	**32.4 ± 7.8**	**37.7 ± 13.4**								
MDA-MB-231 (LUNG1)	**40.2 ± 6.4**	**42.6 ± 6.2**								
MDA-MB-231 (ALN2)	**39.2 ± 5.9**	**40.2 ± 7.4**								

** indicates p-values < 0.01.

cisplatin to result in significant cell kill. Any type of liposomes not containing cisplatin did not result in significant cell kill (Figure A.16 and A.17).

In vitro studies on multicellular spheroids

The interstitium of spheroids- used as surrogates of the tumors' avascular regions -formed of all five cell lines (Figures A.18 A through D) was found to develop pH gradients with the pH decreasing from the spheroid edge (pH ~ 7.2-7.0) towards the core where the average pH value was 6.2 ±0.1.

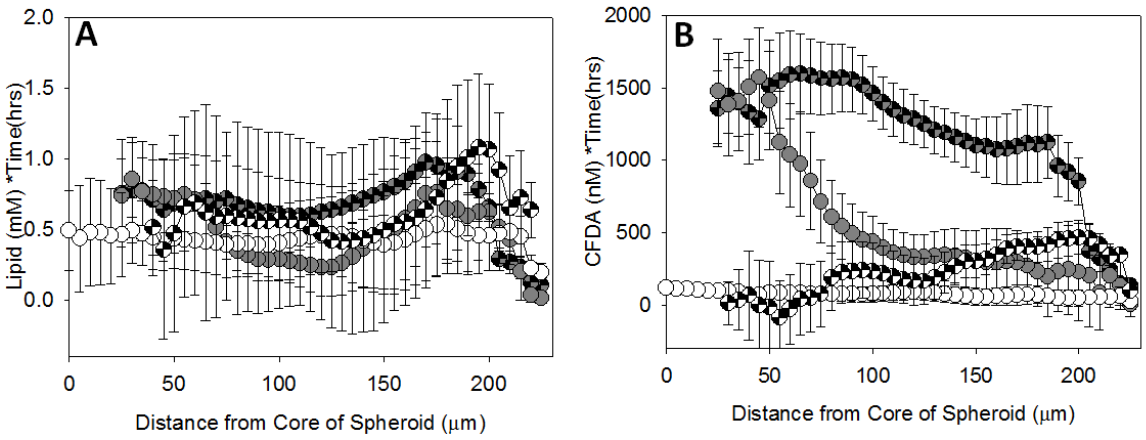

Figure 3.4: Time integrated radial concentrations of lipid (A) and of delivered contents (B) in MDA-MB-231 (ATCC) spheroids. Size of spheroids: 400 ± 40 μm.. Error bars correspond to standard deviations of repeated measurements. 5-8 spheroids per time point; 5 time points Grey checkered circles: pH-releasing liposomes with DAP, grey circles: pH-releasing liposomes without DAP, white checkered circles: non-pH-releasing liposomes with DAP, white circles: non-pH-releasing liposomes without DAP.

The spatiotemporal profiles within spheroids of the different types of liposomes and their contents were affected by the pH-dependent effective charge of liposomes and/or by the pH-releasing property of liposomes, respectively. In particular, for a 6-hour incubation of spheroids with liposomes followed by removal of liposomes from

suspension medium, the time integrated radial lipid concentrations were generally greater for liposomes containing DAP compared to liposomes not containing DAP (Figure 3.4A). The kinetic profiles suggested that this was mostly due to the slower liposomes 'clearance' and not due to the greater 'uptake' of the DAP-functionalized liposomes; where 'uptake'('clearance') refers to the spatiotemporal profiles in the presence (in the absence) of liposomes in the media surrounding the spheroids. This slower clearance was attributed to the cationic charge on these liposomes which should have increased at radii closer to the spheroid core (extent up liposome uptake and clearance individually, Figure A.19) resulting mostly in liposomes' electrostatic adsorption to (and not internalization by) cells and also, possibly, in liposome binding to the ECM that is reported to exhibit areas of negative charge [64, 65].

Similarly, the time integrated radial concentrations of the platinum surrogate delivered by liposomes (Figure 3.4B) exhibited the following order (particularly in the inner half-volume of spheroids, $0 \leq r \leq 100$ μm): adsorbing liposomes with interstitial content release > non-adosrbing liposomes with interstitial content release > adsorbing liposomes without interstitial content release > non-adsorbing liposomes without interstitial content release.

The control of spheroid growth and outgrowth following incubation with all liposomal constructs is shown on Figures 3.5A to D. In all cases, the free agent, cisplatin, exhibited the best efficacy followed - in all cell lines and sub-lines tested - by exactly the same order as the order measured in Figure 3.4B for the time integrated content concentrations, namely: adsorbing liposomal cisplatin with interstitial cisplatin release > non-adsorbing liposomal cisplatin with interstitial cisplatin release > adsorbing

liposomal cisplatin without interstitial cisplatin release > non-adsorbing liposomal cisplatin without interstitial cisplatin release.

Evaluation of growth control of TNBC metastases in vivo

The metastatic animal model studied herein [70] was found to be especially aggressive resulting in fast growth of tumor burden - mainly due to growth of the primary orthotopic tumor - demanding animal sacrifice only a few days after detection of metastatic sites by imaging. In order to allow more time to potentially study the effect on growth control of metastases of the different therapeutic modalities, the primary tumor was completely resected, and the growth of metastases was followed over time.

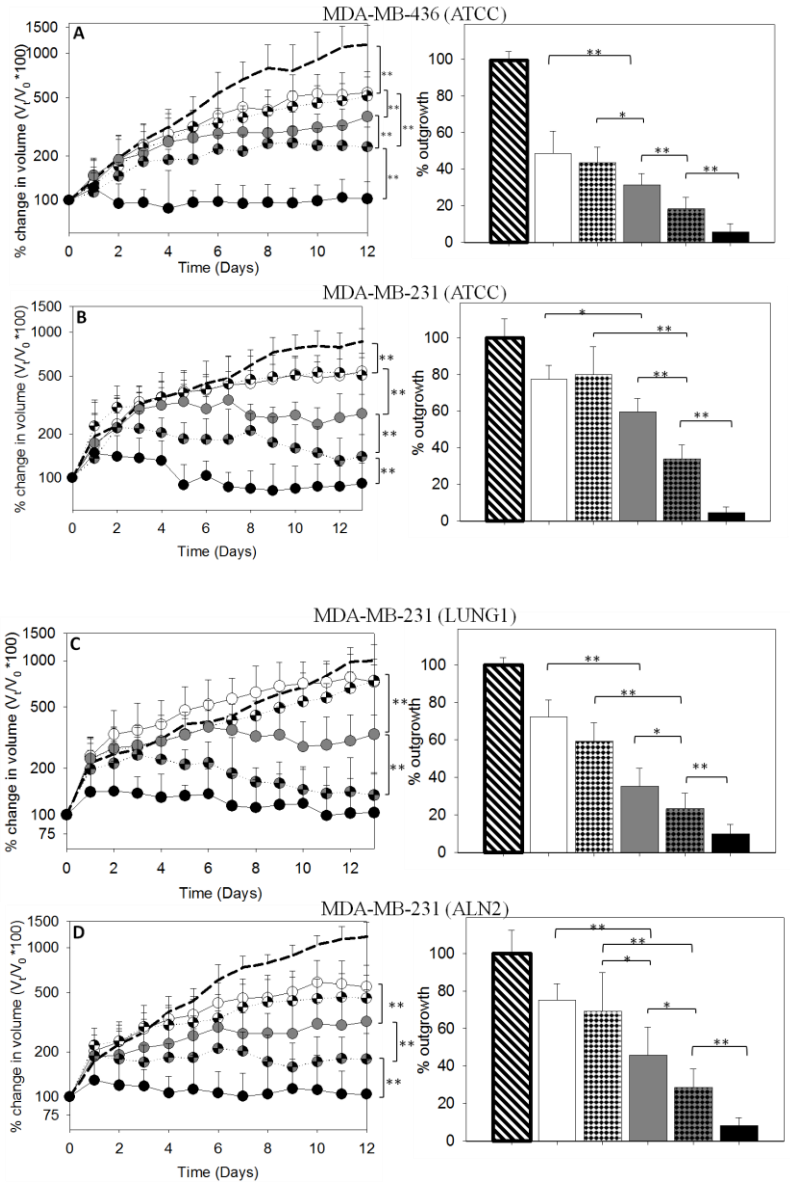

Figure 3.5: Left: Growth control of multicellular spheroids. Treated with pH-releasing liposomes with DAP (grey checkered circles), pH-releasing liposomes without DAP (grey circles), non-pH-releasing liposomes with DAP (white checkered circles), non-pH-releasing liposomes without DAP (white circles), and free cisplatin (black circles). No treatment spheroids are indicated by a thick dashed line. **Right:** Percent spheroid outgrowth. Pattern and colors agree with constructs shown on left; no treatment spheroids shown in white bar with thick black diagonal pattern. (A) MDA-MB-436 (ATCC) spheroids treated with 35 µM of cisplatin in all forms, (B) MDA-MB-231 (ATCC) spheroids treated with 150 µM cisplatin in all forms, (C) MDA-MB-231 (LUNG1) spheroids treated with 150 µM cisplatin in all forms, (D) MDA-MB-231 (ALN2) treated with 150 µM cisplatin in all forms. Error bars correspond to standard deviations of repeated measurements: 2 independent runs were performed; 6-8 spheroids per construct per run. ** indicates p-values < 0.01. * indicates p-values $0.01 < p < 0.05$.

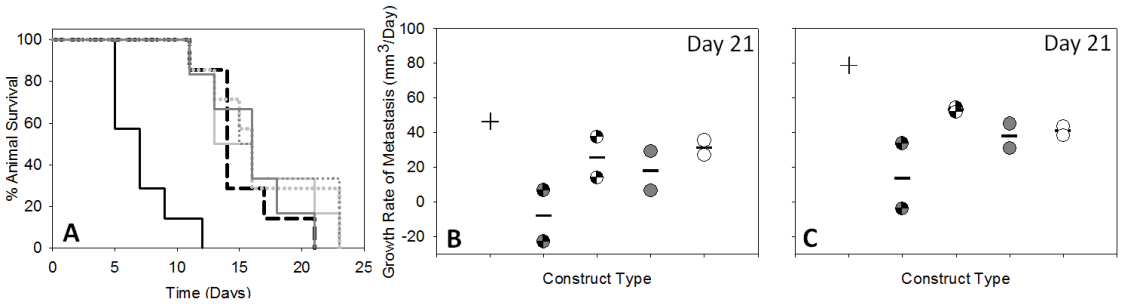

Figure 3.6: Survival plot (A) of mice treated with pH-releasing liposomes with DAP (dotted dark grey line), pH-releasing liposomes without DAP (solid dark grey line), non-pH-releasing liposomes with DAP (dotted light grey line), non-pH-releasing liposomes without DAP (solid light grey line, free cisplatin (solid black line) or no treatment (thick dashed line). Growth rate (B) of single major metastasis and (C) total metastatic burden (all metastasis volumes summed) on Day 21 after beginning treatment. pH-releasing liposomes with DAP (grey checkered circles), pH-releasing liposomes without DAP (grey circles), non-pH-releasing liposomes with DAP (white checkered circles), non-pH-releasing liposomes without DAP (white circles), and free cisplatin (black circles). 5-7 animals per construct.

Figure 3.6A (survival plot) shows that all animal groups which received any of the liposomal forms of cisplatin had a small population of individuals which exhibited longer survival compared both to animals that received free cisplatin and to animals that did not receive any treatment. The administration of same doses of cisplatin in its free form resulted in acute deaths due to drug toxicities. By day 11 upon initiation of therapy at which all mice treated with free cisplatin were sacrificed, fifty percent of animals in all other categories were still alive. Comparison of the volume growth rate of the sum of all observable metastases over time (Figure 3.7) or the volume growth rate of the main metastatic site (Figure A.20) over time also demonstrated favorable trends from animals administered the liposomal cisplatin which was labeled with the adsorptive switch independent of the liposomal property of interstitial content release. The significance of this finding could be related on the actual tumor environment which - given its variety of innate enzymatic contents [71] - may be particularly destabilizing to the liposome

membrane inducing, therefore, interstitial release of encapsulated contents even in the absence of a triggered release property; we have previously demonstrated this effect on liposomes using the secretory phospholipase A_2 (PLA2) *in vitro* [72].

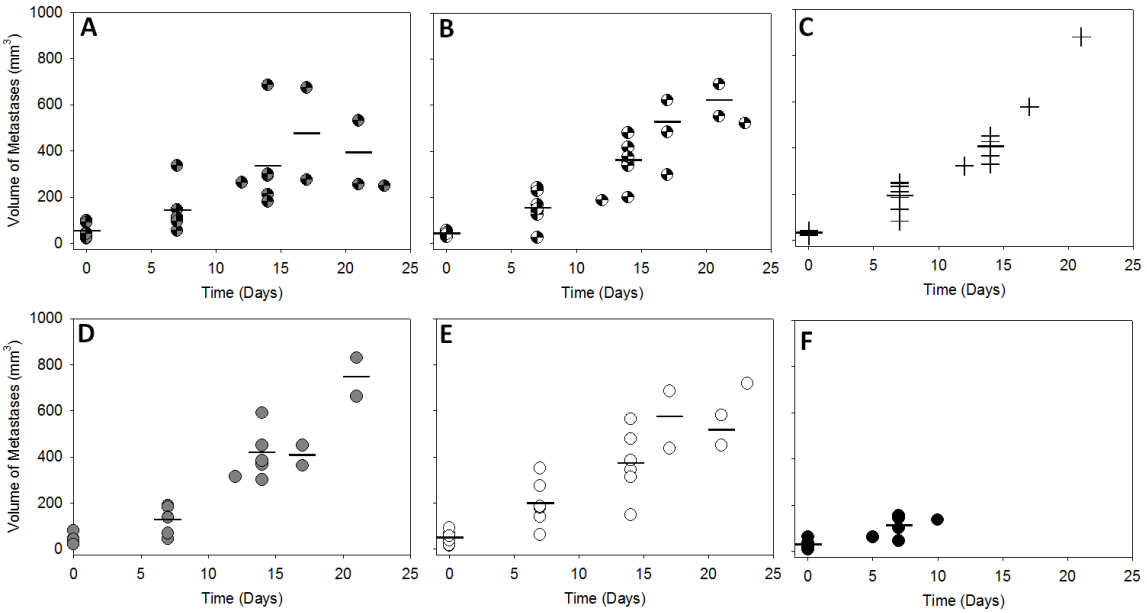

Figure 3.7: Total metastatic burden (volume of all metastases summed) in mice vs. time. pH-releasing liposomes with DAP(A), non-pH-releasing liposomes with DAP (B), no treatment (C), pH-releasing liposomes without DAP (D), non-pH-releasing liposomes without DAP (E), and free cisplatin(F).

Given the aggressiveness of the particular animal model, *the extent of suppressing the rate* of metastatic growth was suggested as an appropriate metric for comparing the effect of the various processes (adsorption, release) whose effect was clearly detected *in vitro*, in spheroids. In particular, Figure 3.6B and C demonstrate that the animals that survived the longest were characterized by the greatest dissipation of metastatic growth which was achieved by administration of the adsorbing liposomal cisplatin with interstitial cisplatin release.

3.4: Discussion

Triple negative breast cancers (TNBCs) are associated with poor prognosis due to high proliferation and reoccurrence outside the breast [3, 7] combined with lack of effective therapeutic modalities [49]. A therapeutic modality that may improve efficacy at the sites of metastatic TNBC tumors by better controlling tumor growth, without affecting toxicities, would be of great significance.

In this study, we developed and evaluated the efficacy of a liposomal chemotherapy that aimed to address two factors which are long understood to be critical in improving the therapeutic effects against vascularized (solid) tumors. Namely, (1) the concentration and uniformity of the spatial distribution profiles of therapeutics within tumors [54], and (2) the length of exposure of tumors to these therapeutics. Together, these factors may cooperatively increase the drug's AUC for the majority of cells comprising the tumors, in other words, enhancing the total drug exposure over time.

We previously reported [55, 56] an approach to enable uniform intratumoral drug distributions by inducing release of therapeutics within the tumor interstitium from nanocarriers not internalized by cells following tumor localization. This approach relied on the nanometer size of the carriers utilizing the EPR effect to enable preferential uptake by the tumors. However, to effectively translate this strategy *in vivo*, the intratumoral residence times of such drug-loaded nanocarriers should be at least of a certain duration determined by the rates of drug release from the carriers, by the diffusion-limited transport in the tumor interstitium experienced by the released therapeutic agents, and by the blood clearance kinetics of the nanocarriers that, in turn, affect their tumor clearance.

In the present study, given the relatively fast blood clearance of nanometer sized particles, to increase the nanocarriers' tumor residence times, we introduced an 'adsorptive/adhesive switch' on the nanocarrier surface with the aim to slow down their tumor-clearing kinetics. The switch was designed to primarily promote adsorption of nanocarriers on cancer cells and/or the ECM while keeping their internalization by cells to a minimum.

In this study, the composition of pH-releasing liposomes was chosen to exhibit the optimum behavior between fast and extensive content release in slightly acidic pH and stable retention of contents in physiological pH. Certainly the drug and nanocarrier diffusivities in the interstitium of actual metastatic tumors and of 3D multicellular spheroids were not expected to be same. However, given the complexity of additional factors *in vivo* (e.g. circulation times, tumor delivered doses, etc.), it is noteworthy that the significance of these properties was also - to some extent - demonstrated i*n vivo*.

Both mechanisms - of promoting drug spreading in the tumor and of slow clearance from the tumor - were chosen to be activated in the slightly acidic pH of the tumor interstitium. Notably, the pH-triggered properties are especially appropriate for TNBC given that acidification of the tumor microenvironment (due to extracellular acidosis via enhanced glycolysis) is common on tumors of patients with TNBC [73], and is correlated with highly aggressive tumors [58, 74, 75].

Tumor selective uptake in this study was expected to be mediated by the EPR effect by using liposomes whose clearance was tuned by their gel-phase membranes [76] and extensive PEGylation [77, 78]. It is well understood that the EPR effect is generally accepted and experimentally confirmed in animal models - and is associated

with the relatively fast growth of tumor formation. However in humans, only certain types of tumors have been shown to exhibit this property. The findings of recent clinical trials using liposomal chemotherapy [79] emphasize exactly this point: the significance of patient pre-screening using probe liposomes (or other nanocarriers) to confirm EPR-mediated nanoparticle uptake by tumors so as to better define the appropriate target group that will benefit the most of such therapeutic modalities.

In this study, we demonstrated that the slow tumor clearance has the potential to significantly suppress the rate of growth of metastatic TNBC tumors *in vivo*. The animal model used in this study was found to be too aggressive to help identify effects of the different modalities on the duration of animal survival. As stated above, the intrinsic aggressiveness of the animal model may have hindered the clear demonstration of the greater effectiveness of the two properties which were clearly shown to play critical roles in model tumor surrogates *in vitro*. Additional reasons could have been due to the actual tumor microenvironments being different from those of the spheroids *in vitro*. Ongoing studies on systematic intratumoral spatiotemporal profiles from these actual metastases are aimed to enable us to identify such differences with the goal of optimizing these constructs. These studies may enable correlation of the tumor microenvironment and transport profiles of the delivered therapeutics to the small population of animals treated with adsorptive/releasing liposomes and which exhibited longer survival, so as to better understand the optimal *in vivo* conditions and to better identify target groups which would benefit more from this type of therapeutic modality.

CHAPTER 4: DISSERTATION SUMMARY

4.1: Significant Findings

The goal of this dissertation was to develop an environmentally tunable liposomal composition loaded with chemotherapy and investigate its ability to treat metastatic TNBC. In Chapter 2, a pH-releasing liposome loaded with cisplatin was developed and tested in vitro to determine efficacy against TNBC 2D monolayers and 3D multicellular spheroids. pH-releasing liposomes were shown to be the superior liposomal composition, compared to non-pH-releasing liposomes, when incubated with cells at acidic pH. The heightened release of the contents of the liposomes in diffusion limited 3D spheroids, led to enhanced penetration of the drug, shown in the penetration profiles, and better growth control and lower percent outgrowth.

While the *in vitro* results in Chapter 2 were promising, *in vivo* studies are more appropriate in determining the efficacy of the treatment. They are more challenging as the circulation time of the liposomes in the blood, and the retention time of the liposomes at the tumor, if too short, will lead to ineffective treatment. Chapter 3 investigated a liposome composition functionalized with a PEGylated lipid whose PEG-chain end, DAP, becomes positive at acidic pH leading to cell adsorption compared to liposomes without the PEG-DAP. This allowed for greater retention of the liposomes at the tumor site, to subsequently lead to greater penetration and accumulation of the released drug throughout the tumor, i.e. in more uniform intratumoral drug distributions. Clearance profiles of the liposome carrier showed greater retention time of the PEG-DAP liposomes in spheroids, which led to greater concentration of contents throughout the spheroid with

the pH-releasing composition. This was in agreement with the better control of spheroid growth with the pH-releasing liposomes with PEG-DAP, compared to the pH-releasing liposomes without PEG-DAP, in all four of the TNBC cell lines evaluated.

Finally, *in vivo* results in Chapter 3 showed that administration of pH-releasing liposomes with the adhesive property (via the PEG-DAP functionalization) led to slower growth kinetics of metastases in a TNBC mouse model when compared to metastases growth rates of mice that received control treatments lacking one of both properties (of interstitial release and/or interstitial adhesion).

4.2: Limitations and Future Studies

The main limitation of this study was the aggressiveness of the mouse model used to determine efficacy in controlling the growth rates of metastases. Due to MRI imaging being the only available way to confirm metastatic legion formation, the start of treatment was limited by the detection limit of the MRI. The smallest metastasis measured was ~10 mm^3 however; the metastasis was present and growing much earlier than we were able to detect it. This led to a limitation in the start date of treatment. Perhaps enhanced survival is unable to be obtained due to the aggressiveness of the metastatic growth and if metastases were detected earlier then treatment would be more effective.

There is also the question if the liposomes were toxic to the mice. This will be evaluated using histopathology analysis in the future, however, at this time, it is unknown. If this is the case, a more applicable treatment regiment should be used. Perhaps lower concentrations of liposomal cisplatin could be administered at shorter time

intervals so the drug concentration within the blood would consistently be within the therapeutic window. Effective treatment of metastatic TNBC with pH-releasing PEG-DAP liposomes, leading to enhanced survival *in vivo*, could be in the near future with further experimental design optimization.

APPENDIX

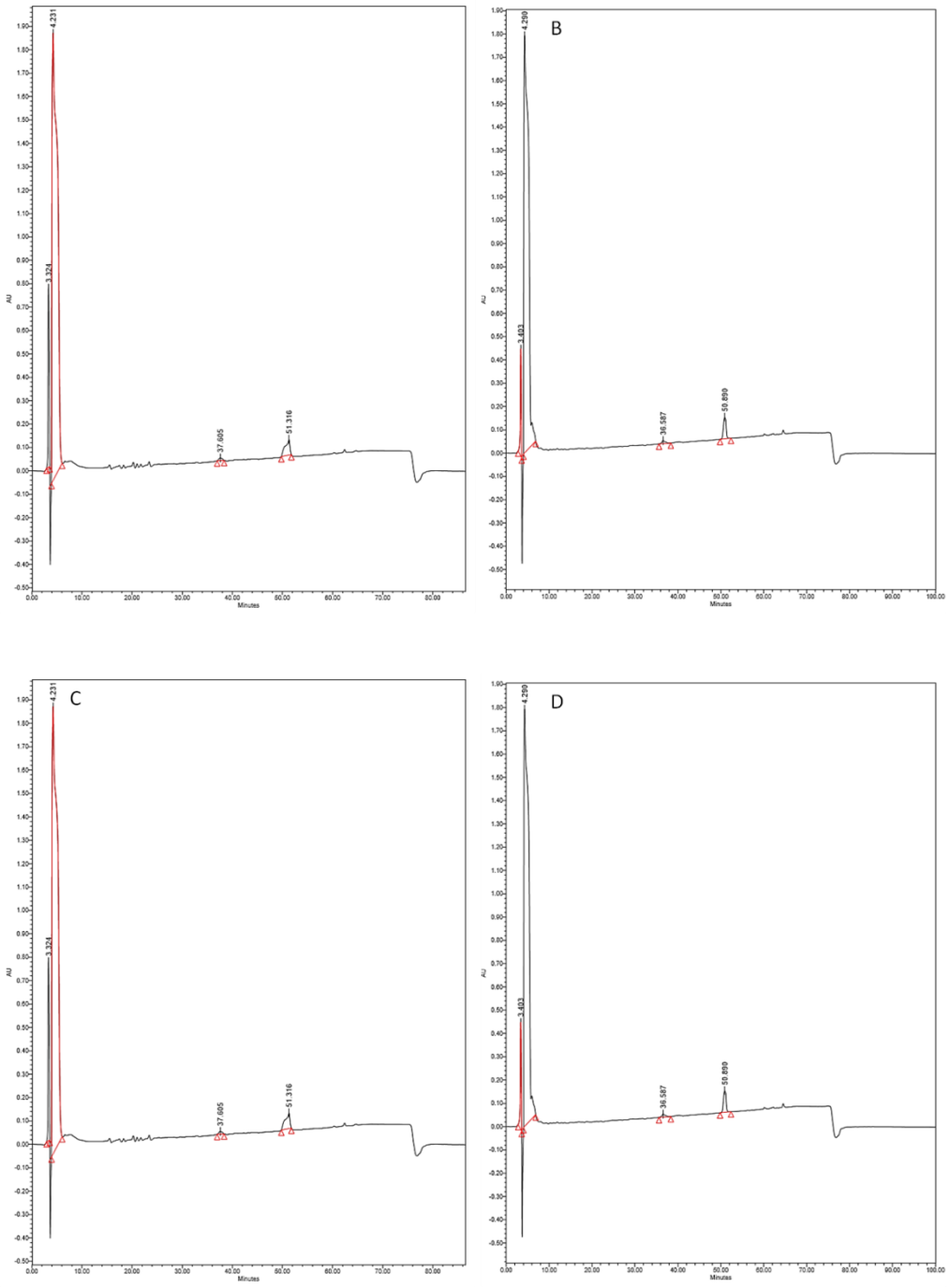

Figure A.1: HPLC results of liposomes being passed through a C8 column. pH-releasing liposomes before (A) and after (B) heating and non-pH-releasing liposomes before (C) and after (D) heating. The heat that liposomes are exposed, 80°C for 4 hours, are consistent with loading conditions. Results show no significant changes in HPLC elution profile.

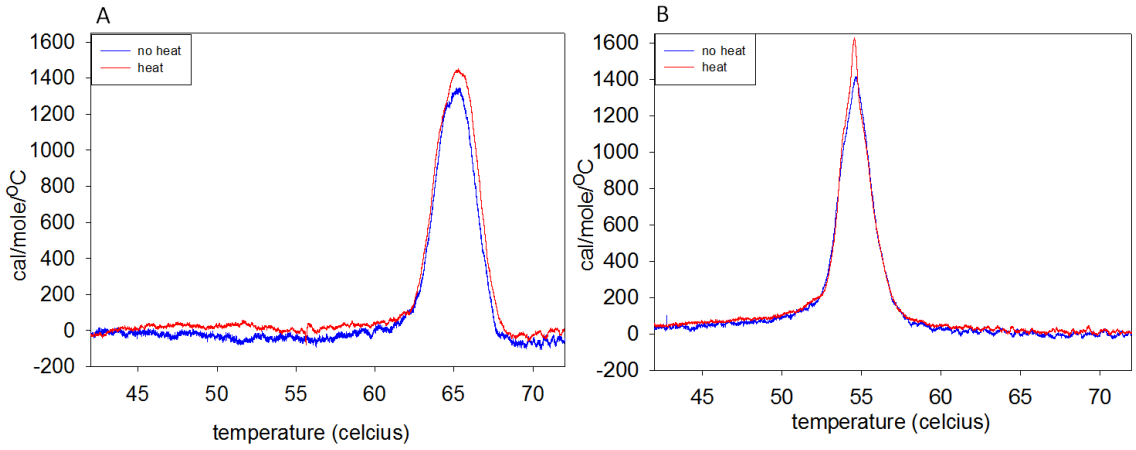

Figure A.2: Dynamic scanning calorimetry (DSC) scans of pH-releasing (A) and non-pH-releasing (B) liposomes to show the lack of effects after exposed the liposomes to the loading conditions which are heating the liposomes at 80°C for 4 hours. Results indicate no significant changes in bilayer before and after heating.

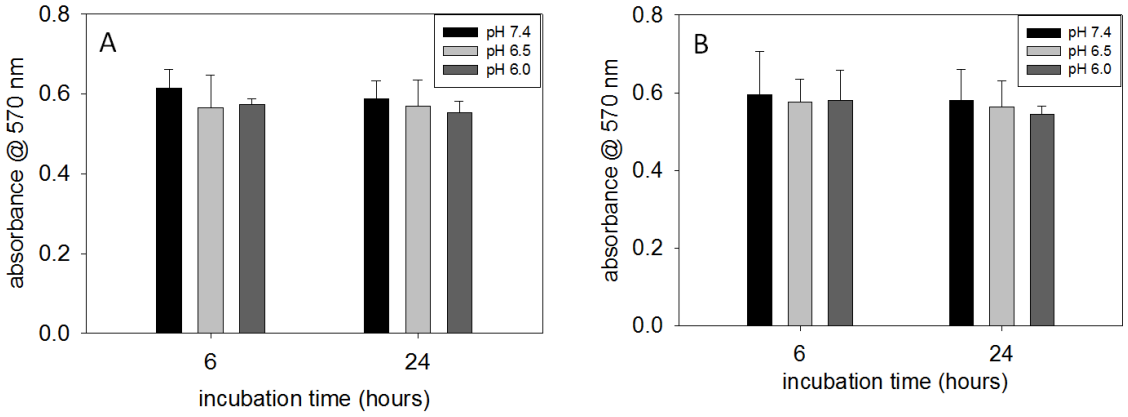

Figure A.3: Absorbance values of MDA-MB-231 (A) and MDA-MB-468 (B) cells after a 24 hour incubation at different extracellular pH values. After incubation, cells are washed with PBS and sit for two doubling times after which an MTT assay is performed and absorbance (570 nm) is read on a plate reader.

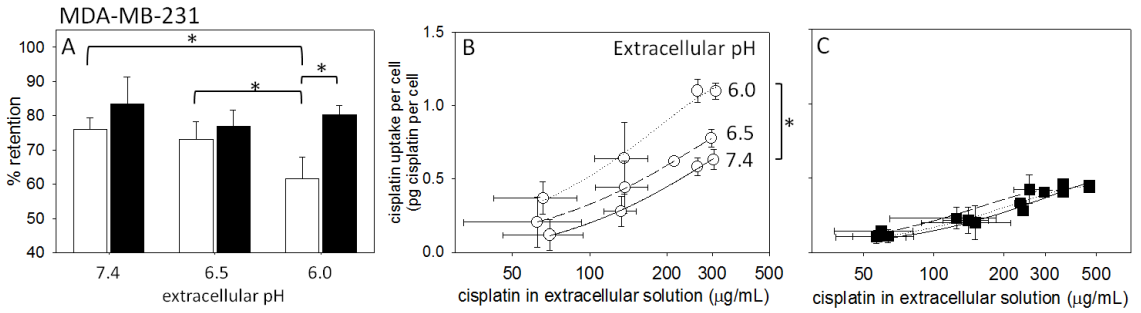

Figure A.4: (A) Retention of encapsulated cisplatin by pH-releasing liposomes (white bars) and non-pH-releasing liposomes (black bars) following 6 hours of incubation with MDA-MB-231 cells. 3 independent liposome preparations per data point. * indicates p-values < 0.05. (B) and (C) Uptake of cisplatin (pg of cisplatin per cell) by MDA-MB-231 cells delivered by pH-releasing liposomes (B) and by non-pH-releasing liposomes (C) following 6 hours of incubation at extracellular pH values of 7.4, 6.5, and 6.0. White circles: pH-releasing liposomes loaded with cisplatin; black squares: non-pH-releasing liposomes loaded with cisplatin. Error bars correspond to standard deviations of repeated measurements. Three independent liposome preparations, 2 samples per preparation. * indicates p-values < 0.05.

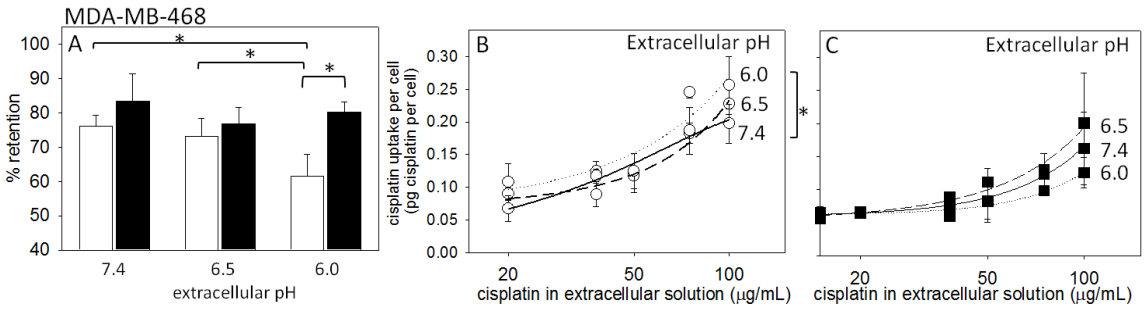

Figure A.5: (A) Retention of encapsulated cisplatin by pH-releasing liposomes (white bars) and non-pH-releasing liposomes (black bars) following 6 hours of incubation with MDA-MB-468 cells. Error bars correspond to standard deviations of repeated measurements. Three independent liposome preparations per data point. * indicates p-values < 0.05. (B) and (C) Uptake of cisplatin (pg of cisplatin per cell) by MDA-MB-468 cells delivered by pH-releasing liposomes (B) and by non-pH-releasing liposomes (C) following 6 hours of incubation at extracellular pH values of 7.4, 6.5, and 6.0. White circles: pH-releasing liposomes loaded with cisplatin; black squares: non-pH-releasing liposomes loaded with cisplatin. Error bars correspond to standard deviations of repeated measurements. Three independent liposome preparations, 2 samples per preparation. * indicates p-values < 0.05.

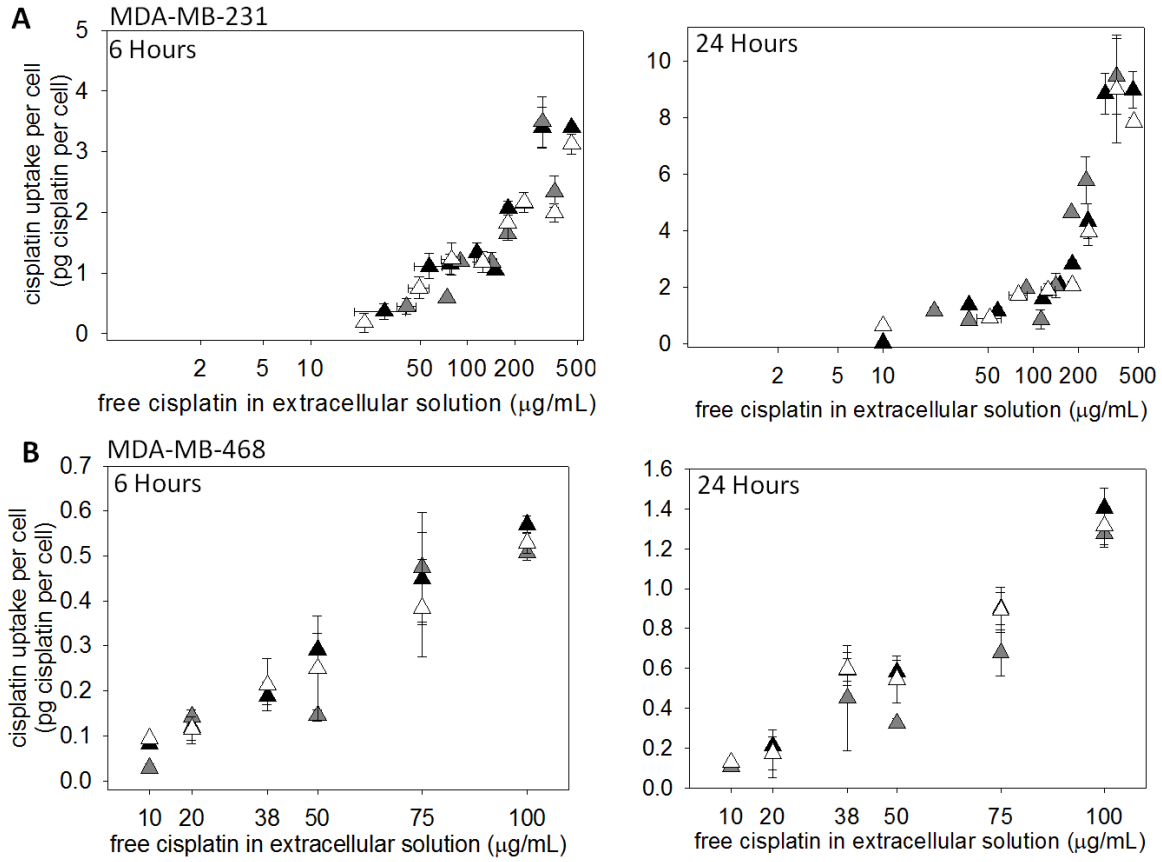

Figure A.6: Uptake of free cisplatin (pg of cisplatin per cell) by (A) MDA-MB-231 cells and (B) MDA-MB468 cells following 6 and 24 hours of incubation at extracellular pH values of 7.4 (black triangles), 6.5 (gray triangles), and 6.0 (white triangles). Error bars correspond to standard deviations of repeated measurements. Three independent measurements per data point.

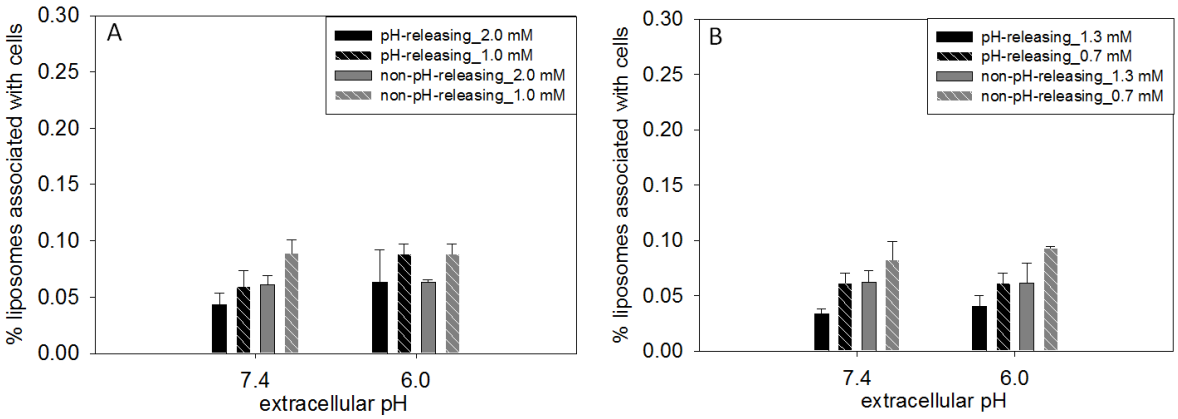

Figure A.7: Liposome cell uptake after a 6-hour incubation of liposomes with MDA-MB-231cells (A) and MDA-MB-468 cells (B) in suspension at 37°C. Liposomes are labeled with Rhodamine and are able to be detected using a fluorometer. After the incubation cells are washed with PBS and lysed. Rhodamine fluorescence (ex. 550, em. 590) is determined before and after washing and the percentt liposomes associated with the cells is determined.

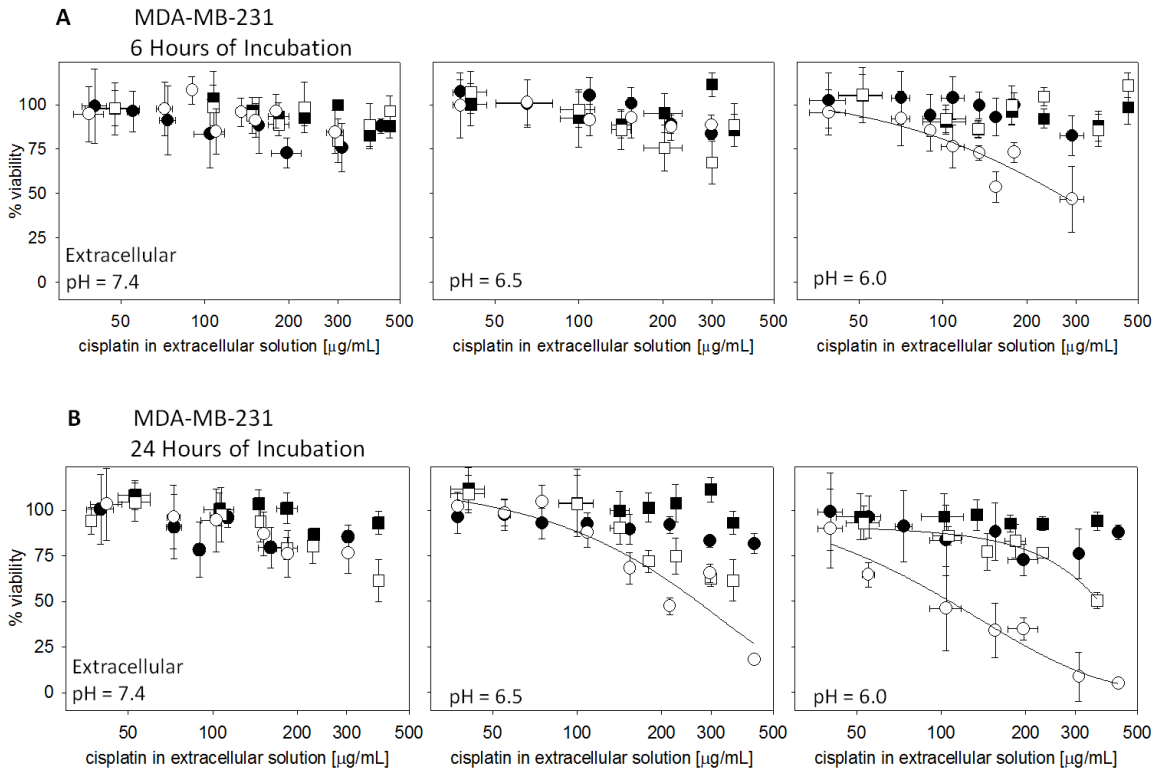

Figure A.8: Dose-response of MDA-MB-231 cells in monolayers to liposomal cisplatin for different extracellular pH (7.4, 6.5, 6.0) and incubation times ((A) 6 and (B) 24 hours). Open (filled) circles: pH-releasing liposomes loaded (not loaded) with cisplatin; open (filled) squares: non-pH-releasing liposomes loaded (not loaded) with cisplatin. Error bars correspond to standard deviations of repeated measurements. Three independent liposome preparations per data point.

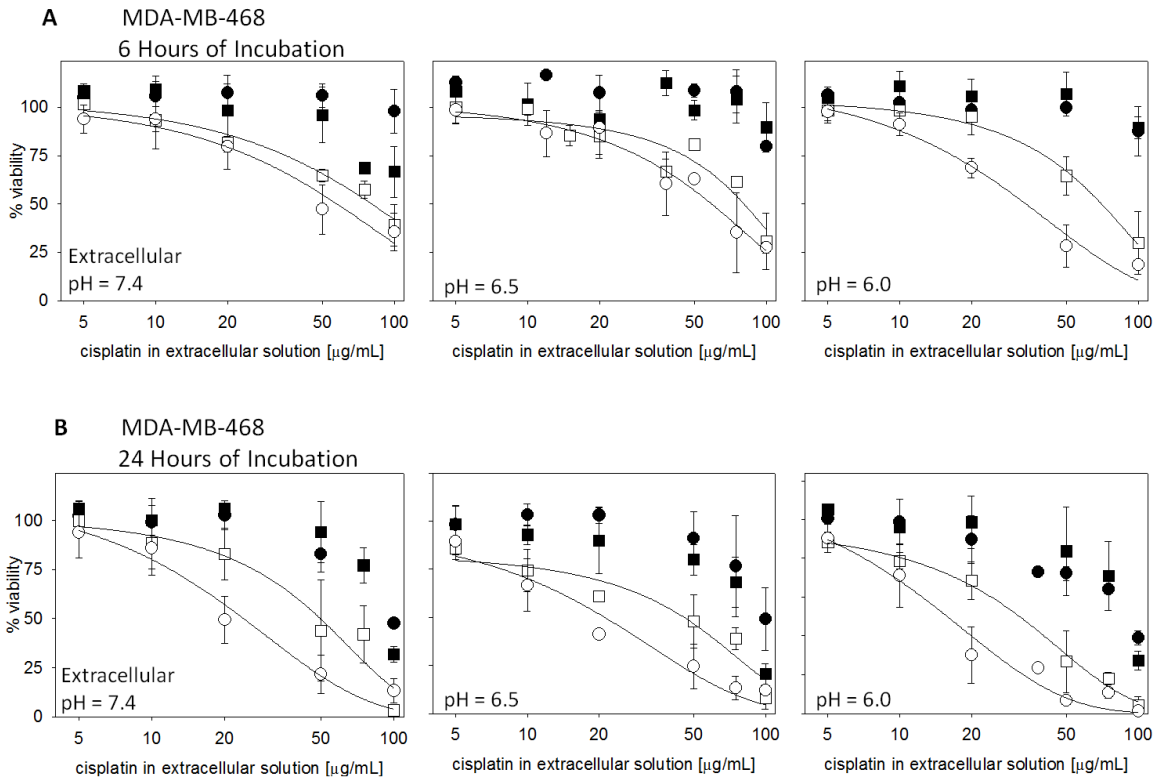

Figure A.9: Dose-response of MDA-MB-468 cells in monolayers to liposomal cisplatin for different extracellular pH (7.4, 6.5, 6.0) and incubation times ((A) 6 and (B) 24 hours). Open (filled) circles: pH-releasing liposomes loaded (not loaded) with cisplatin; open (filled) squares: non-pH-releasing liposomes loaded (not loaded) with cisplatin. Error bars correspond to standard deviations of repeated measurements. Three independent liposome preparations per data point.

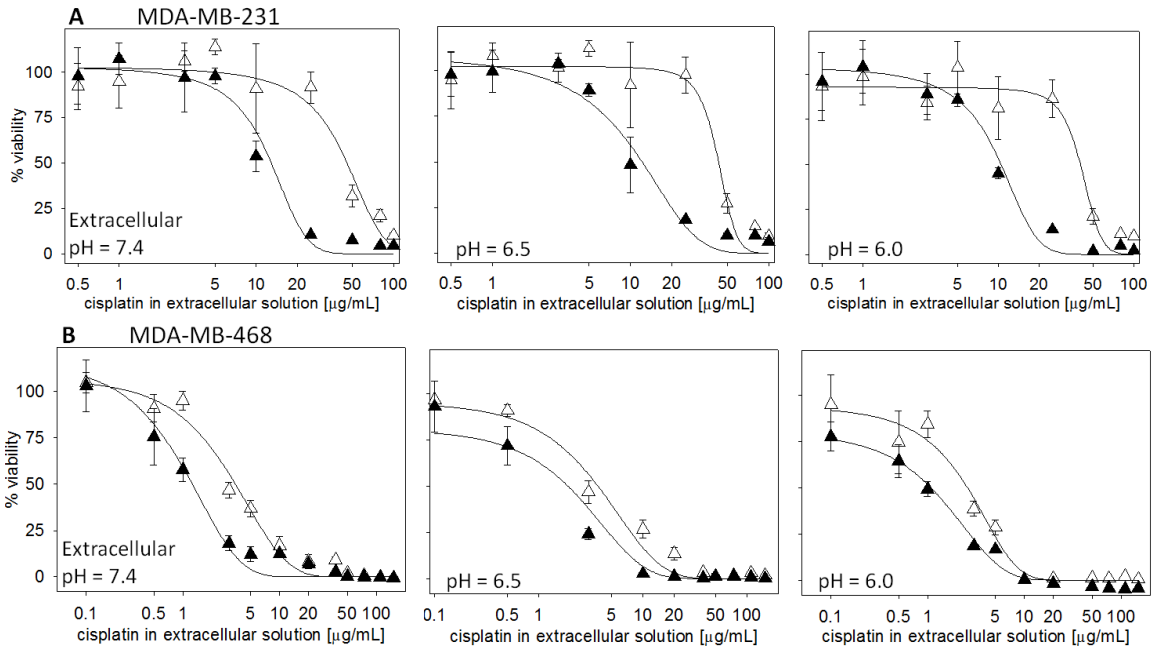

Figure A.10: Dose-response of (A) MDA-MB-231 cells and (B) MDA-MB-468 cells in monolayers to free cisplatin for different extracellular pH (7.4, 6.5, 6.0) and incubation times (6 and 24 hours). White (black) triangles: 6 (24) hours of incubation. Error bars correspond to standard deviations of repeated measurements. Three independent liposome preparations per data point.

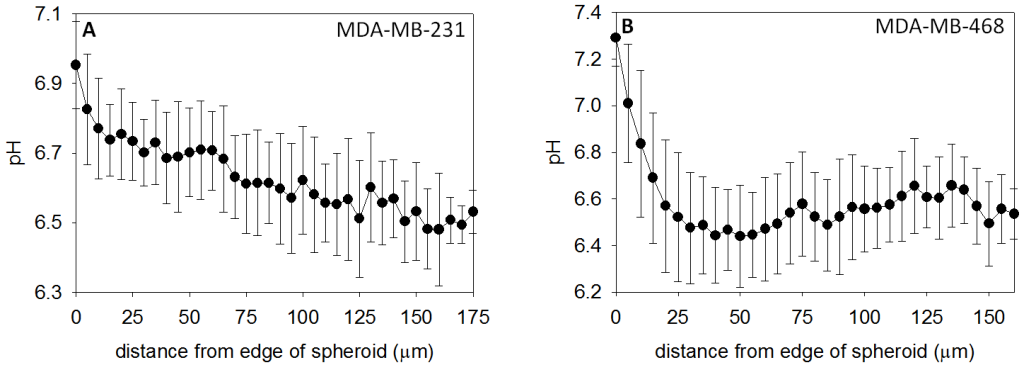

Figure A.11: Interstitial pH gradient of MDA-MB-231 (A) and MDA-MB-468 (B) multicellular spheroids. Error bars correspond to standard deviations of measurements averaged over 5 spheroids.

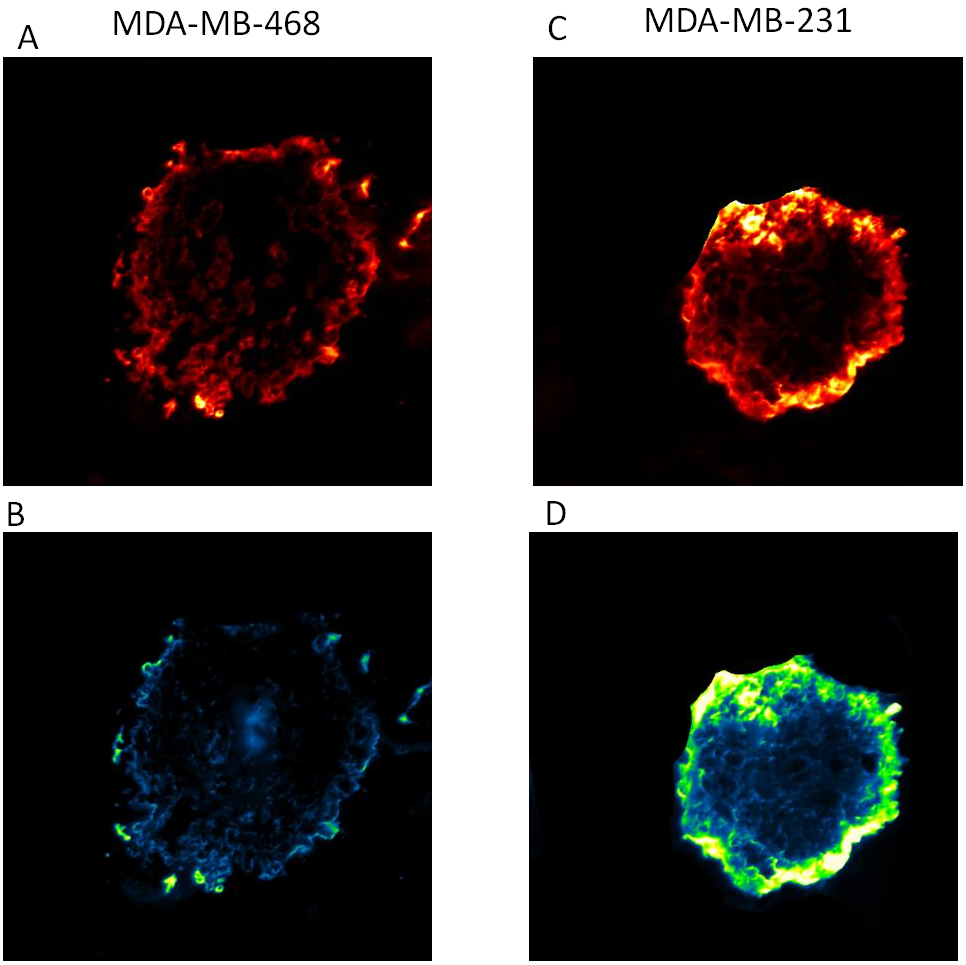

Figure A.12: Characteristic images of spheroids that were sliced and imaged to determine the liposome distribution (A and B) and content distribution (C and D).

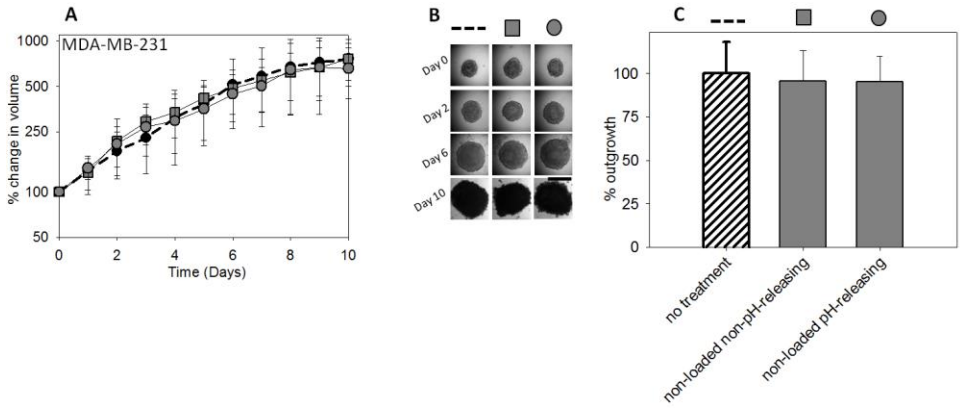

Figure A.13: (A) Control of MDA-MB-231 spheroid growth over time, (B) characteristic images of spheroids during monitoring of growth, and (C) extent of outgrowth of spheroids following the end time point shown in (A). Gray circles: pH-releasing liposomes not loaded with cisplatin; gray squares: non-pH-releasing liposomes not loaded with cisplatin; dashed line: no treatment. Error bars correspond to standard deviations of repeated measurements. Two independent liposome preparations, 7 spheroids per treatment type per preparation. No statistically different changes were observed in % change in volume = V_t/V_o x 100%, where V_t is volume at time t and V_o volume before addition of liposomes. At t = 0 the average volume of spheroids was 300 $\pm$ 50 µm (n = 14 spheroids). Scale bar corresponds to 400 µm.

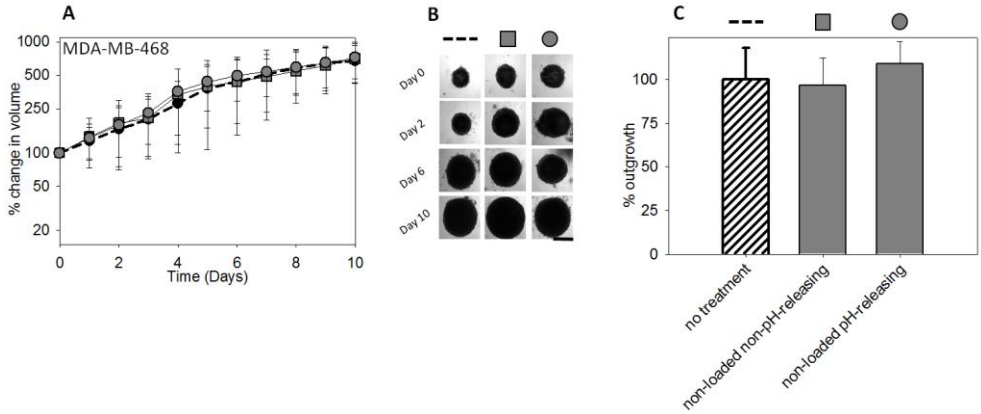

Figure A.14: (A) Control of MDA-MB-468 spheroid growth over time, (B) characteristic images of spheroids during monitoring of growth, and (C) extent of outgrowth of spheroids following the end time point shown in (A). Gray circles: pH-releasing liposomes not loaded with cisplatin; gray squares: non-pH-releasing liposomes not loaded with cisplatin; dashed line: no treatment. Error bars correspond to standard deviations of repeated measurements. Two independent liposome preparations, 7 spheroids per treatment type per preparation. No statistically different changes were observed in % change in volume = V_t/V_o x 100%, where V_t is volume at time t and V_o volume before addition of liposomes. At t = 0 the average volume of spheroids was 300 $\pm$ 50 µm (n = 14 spheroids). Scale bar corresponds to 300 µm.

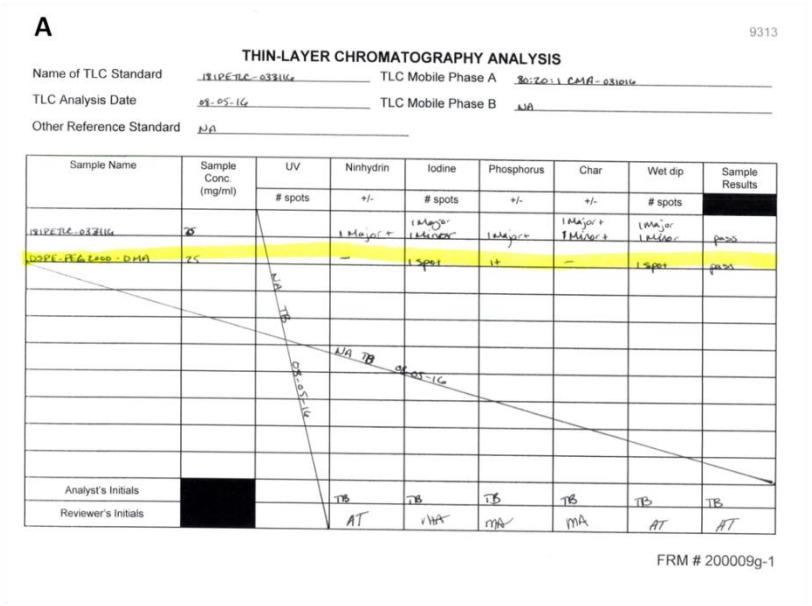

A

9313

THIN-LAYER CHROMATOGRAPHY ANALYSIS

Name of TLC Standard: 18:1PE-TLC-033116 — TLC Mobile Phase A: 80:20:1 CMA-031016

TLC Analysis Date: 08-05-16 — TLC Mobile Phase B: NA

Other Reference Standard: NA

Sample Name	Sample Conc. (mg/ml)	UV # spots	Ninhydrin +/-	Iodine # spots	Phosphorus +/-	Char +/-	Wet dip # spots	Sample Results
18:1PE-TLC-033116	25		1 Major +	1 Major 1 Minor	1 Major +	1 Major + 1 Major +	1 Major 1 Minor	pass
DSPE-PEG2000-DMA	25		—	1 spot	+	—	1 spot	pass
Analyst's Initials			TB	TB	TB	TB	TB	TB
Reviewer's Initials			AT	MA	MA	MA	AT	AT

NA TB 08-05-16

NA TB 08-05-16

FRM # 200009g-1

B

1. 18:1PE-TLC-033116

2. DSPE - PEG2000-DMA

TB 08.05-16

C

Shift (ppm)	Actual Protons	Theoretical Protons	Assignment
Not detected	0.0000	4	NH_4^+
Not detected	0.0000	2	NH
5.23	0.9943	1	proton on C2 of glycero backbone
4.41	1.0469	1	proton on C1 of glycero backbone
4.18	3.2688	3	$PO_4CH_2CH_2NH$- + proton on C1 of glycero backbone
4.07	29.1081	0	water
3.97	2.1712	2	protons on C3 of glycero backbone
3.93	2.3725	2	PEG related
3.83	1.2837	0	PEG satellite
3.68	5.1229	5	PEG related
3.66	183.9913	173	$PO_4CH_2CH_2NH$- + PEG
3.55	2.3025	2	β protons of DMA
3.48	1.1588	0	PEG satellite
3.39	11.1531	4	α protons of DMA + CH_2-NH of PEG + methanol-d4
3.05	0.2543	0	unknown
2.95	0.2170	0	unknown
2.66	6.6912	6	methyl groups of DMA
2.32	4.0047	4	α protons on 18:0 chains
1.60	4.0149	4	β protons on 18:0 chains
1.26	56.2496	56	remaining methylene protons
0.88	6.0000	6	terminal methyl protons

	Actual Sum Protons	Theoretical Sum Protons
Note: Sum excludes PEG satellites and unknowns	289.384	275

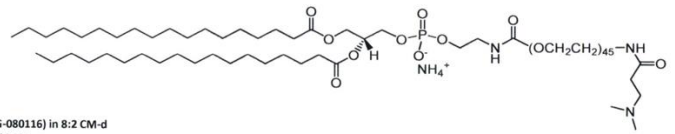

^{1}H NMR of DSPE-PEG2000-DMA (LG-080116) in 8:2 CM-d
Performed by Lolli Meeks on 08/05/2016

Shift (ppm)	Assignment
0.21	PE

^{31}P NMR of DSPE-PEG2000-DMA (LG-080116) in 8:2 CM-d
Performed by Lolli Meeks on 08/05/2016

Figure A.15: TLC experimental conditions (A) and results (B) of custom synthesis of 18:0 PE-PEG-DAP molecule indicating purity >99%.NMR Results (C) of custom synthesis of 18:0 PE-PEG-DAP molecule indicating purified molecule is desired structure

Table A.1: Cell line characterization.

Subline	Mouse #	Metastatic Site	Doubling Time (hrs)
MDA-MB-231 (PRI3)	3	Primary Tumor	26.1 ± 1.7
MDA-MB-231 (LUNG1)	1	Lung	25.1 ± 0.4
MDA-MB-231 (ALN2)	2	Axillary Lymph Node	26.5 ± 0.2
MDA-MB-231 (ATCC)	N/A	N/A	34.8 ± 1.3
MDA-MB-436 (ATCC)	N/A	N/A	41.0 ± 1.9

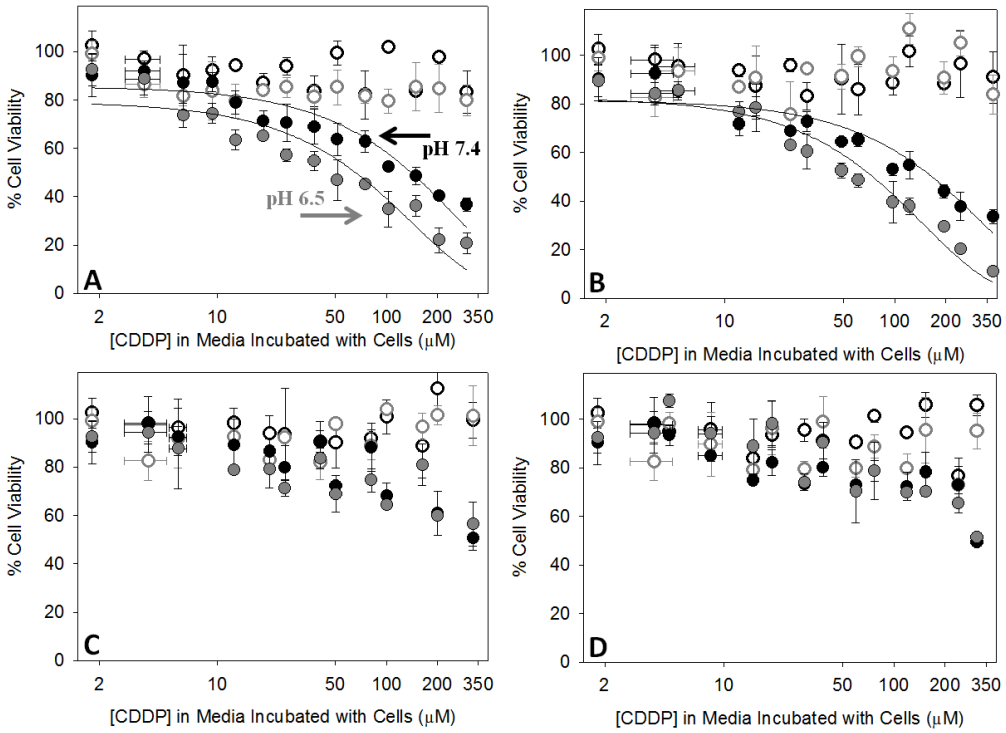

Figure A.16: Dose response of MDA-MB-436 (ATCC) monolayers to different types of liposomal cisplatin (CDDP) after a 6-hour incubation. pH-releasing liposomes with DAP (A), pH-releasing liposomes without DAP (B), non-pH-releasing liposomes with DAP (C), and non-pH-releasing liposomes without DAP(D). Black symbols: pH 7.4, grey symbols: pH 6.5. Fill symbols: loaded liposomes, open symbols: empty liposomes.

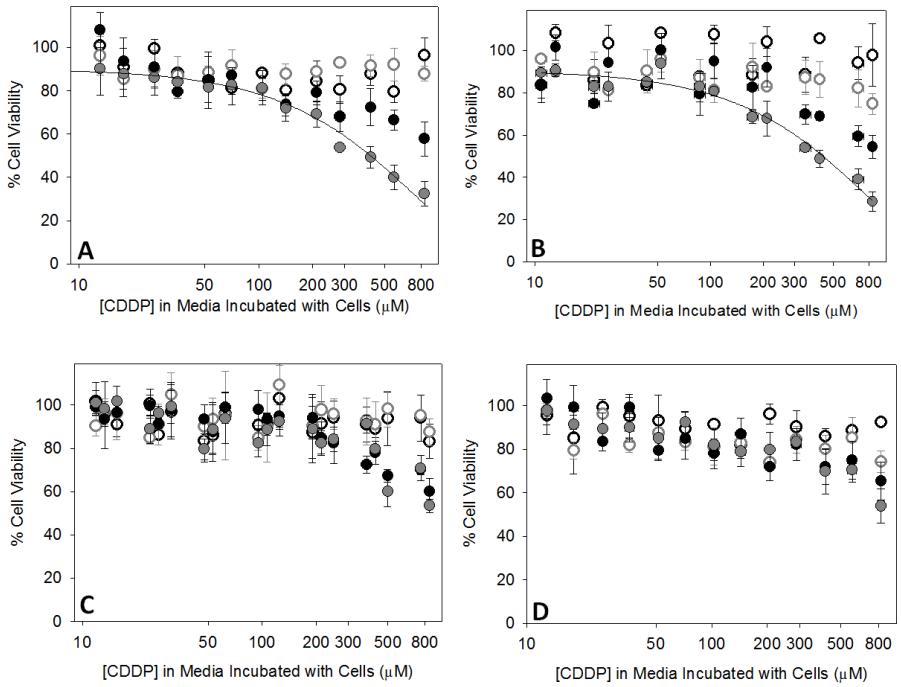

Figure A.17: Dose response of MDA-MB-231 (ATCC) monolayers to different types of liposomal cisplatin (CDDP) after a 6-hour incubation. pH-releasing liposomes with DAP (A), pH-releasing liposomes without DAP (B), non-pH-releasing liposomes with DAP (C), and non-pH-releasing liposomes without DAP(D). Black symbols: pH 7.4, grey symbols: pH 6.5. Fill symbols: loaded liposomes, open symbols: empty liposomes.

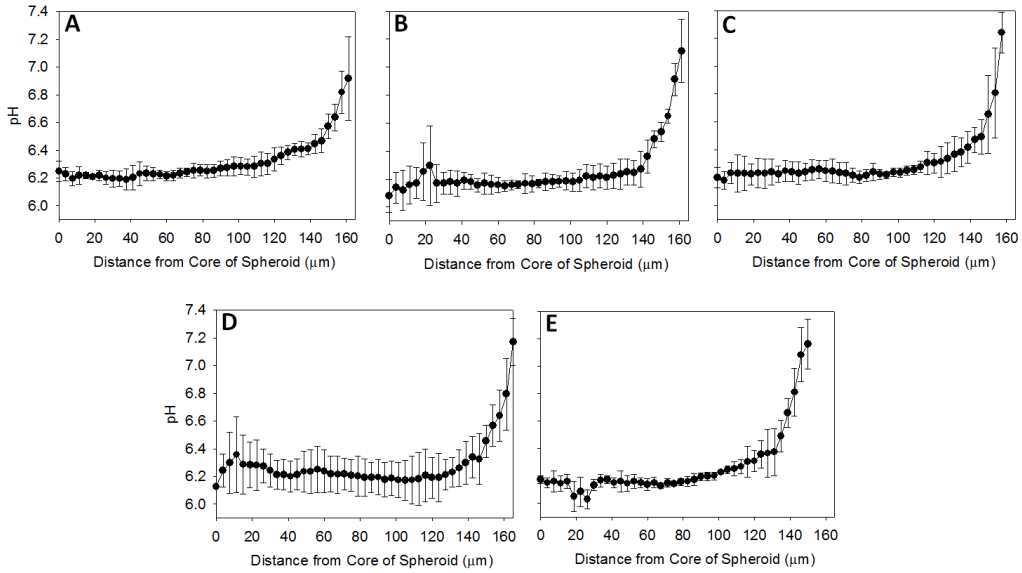

Figure A.18: Interstitial pH gradients of 300 µm-diameter spheroids determined by SNARF-4F. MDA-MB-436 (ATCC) (A), MDA-MB-231 (ATCC) (B), MDA-MB-231 (PRI3) (C), MDA-MB-231(LUNG1) (D), and MDA-MB-231 (ALN2) (E). 5-6 different spheroids analyzed per graph.

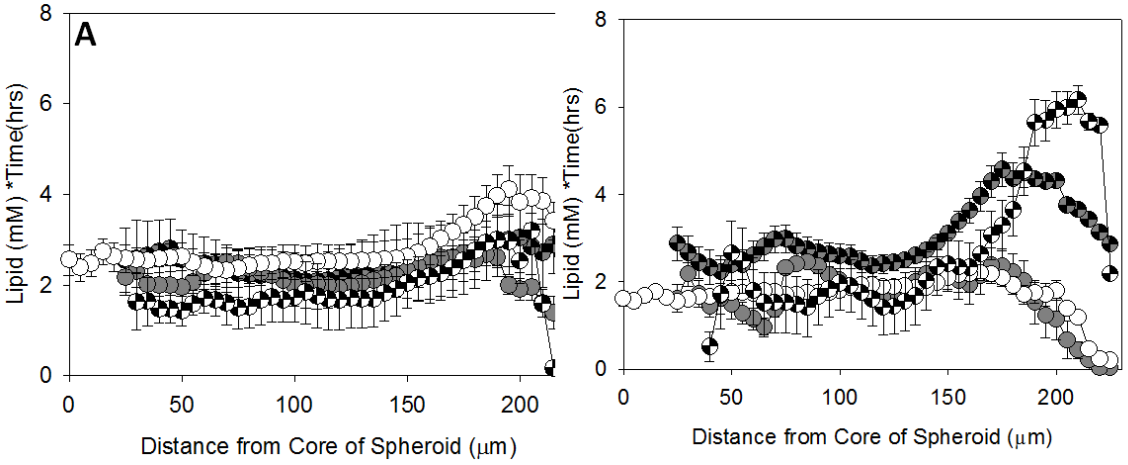

Figure A.19: Time integrated radial concentrations of liposome 'uptake' (A) and liposome 'clearance' (B) in MDA-MB-231 (ATCC) spheroids. Uptake is integrated over 6 hours, and clearance is integrated over 24 hours after spheroids are removed from wells of liposomes. Size of spheroids: 400 ± 40 μm. 5-8 spheroids per time point; 3 time points for uptake and 5 time points for clearance. Error is propogated across all timepoints. Grey checkered circles: pH-releasing liposomes with DAP, grey circles: pH-releasing liposomes without DAP, white checkered circles: non-pH-releasing liposomes with DAP, white circles: non-pH-releasing liposomes without DAP.

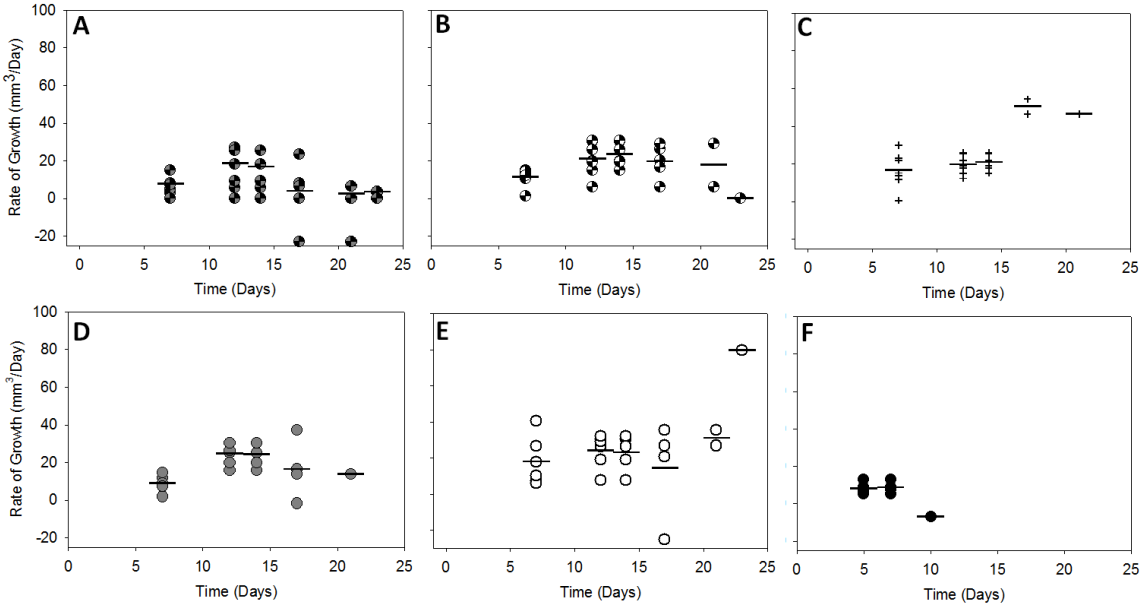

Figure A.20: Growth rate of single major metastasis in mice that received pH-releasing liposomes with DAP (A), non-pH-releasing liposomes with DAP (B), no treatment (C), pH-releasing liposomes without DAP (D), and non-pH-releasing liposomes without DAP (E), and free cisplatin (F).

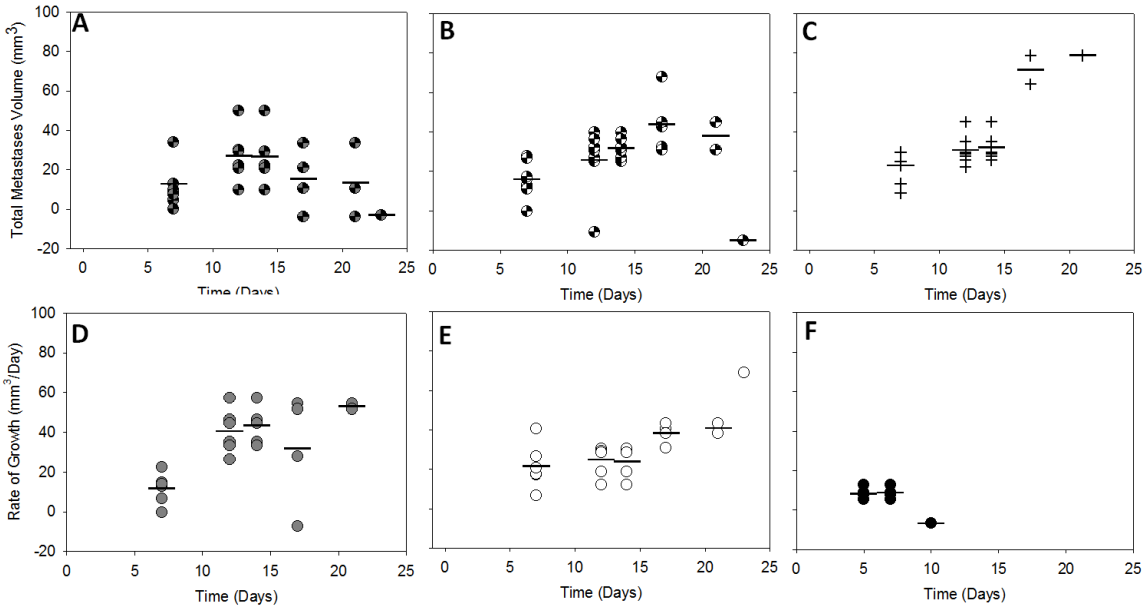

Figure A.21: Growth rate of total metastatic burden in mice that received pH-releasing liposomes with DAP (A), non-pH-releasing liposomes with DAP (B), no treatment (C), pH-releasing liposomes without DAP (D), and non-pH-releasing liposomes without DAP (E), and free cisplatin (F).

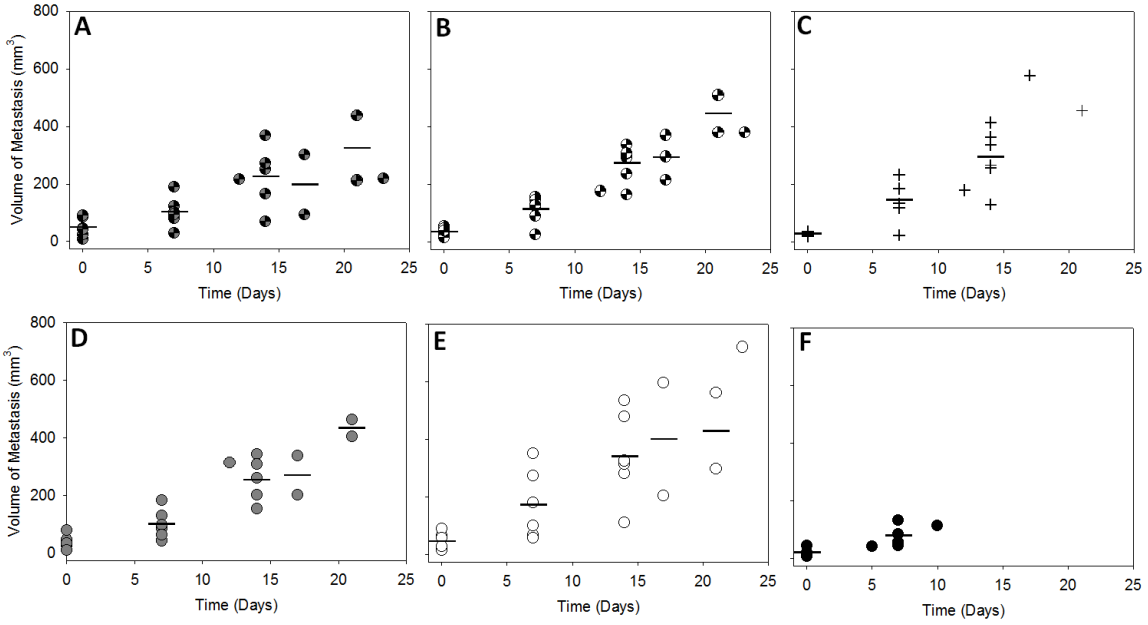

Figure A.22: Volume of single major metastasis in mice vs time that received pH-releasing liposomes with DAP(A), non-pH-releasing liposomes with DAP (B), no treatment (C), pH-releasing liposomes without DAP (D), non-pH-releasing liposomes without DAP (E), and free cisplatin(F).

REFERENCES

[1] Parisi M, Pelletier C, Cherepanov D, Broder MS. Outcomes research examining treatments, quality of life and costs in HER2-negative and triple-negative metastatic breast cancer: a systematic literature review. Journal of comparative effectiveness research. 2018;7:67-83.

[2] Lin NU, Vanderplas A, Hughes ME, Theriault RL, Edge SB, Wong YN, et al. Clinicopathologic features, patterns of recurrence, and survival among women with triple-negative breast cancer in the National Comprehensive Cancer Network. Cancer. 2012;118:5463-72.

[3] Dawood S. Triple-negative breast cancer: epidemiology and management options. Drugs. 2010;70:2247-58.

[4] Mayer IA, Abramson VG, Lehmann BD, Pietenpol JA. New strategies for triple-negative breast cancer--deciphering the heterogeneity. Clinical cancer research : an official journal of the American Association for Cancer Research. 2014;20:782-90.

[5] Duan X, He C, Kron SJ, Lin W. Nanoparticle formulations of cisplatin for cancer therapy. Wiley interdisciplinary reviews Nanomedicine and nanobiotechnology. 2016;8:776-91.

[6] Minchinton AI, Tannock IF. Drug penetration in solid tumours. Nature reviews Cancer. 2006;6:583-92.

[7] Dent R, Trudeau M, Pritchard KI, Hanna WM, Kahn HK, Sawka CA, et al. Triple-negative breast cancer: clinical features and patterns of recurrence. Clinical cancer research : an official journal of the American Association for Cancer Research. 2007;13:4429-34.

[8] Fantini Mea. Triple Negative Breast Cancer Treatment: Use of Platinum and Platinum Analogs. . Journal of Cancer Therapy. 2012;13:4429-34.

[9] Telli M. Optimizing chemotherapy in triple-negative breast cancer: the role of platinum. American Society of Clinical Oncology educational book American Society of Clinical Oncology Meeting. 2014:e37-42.

[10] Anders C, Carey LA. Understanding and treating triple-negative breast cancer. Oncology (Williston Park, NY). 2008;22:1233-9; discussion 9-40, 43.

[11] Kelland L. The resurgence of platinum-based cancer chemotherapy. Nature reviews Cancer. 2007;7:573-84.

[12] Sempkowski M, Locke T, Stras S, Zhu C, Sofou S. Liposome-based approaches for delivery of mainstream chemotherapeutics: preparation methods, liposome designs, therapeutic efficacy. Critical reviews in oncogenesis. 2014;19:177-221.

[13] Liu D, He C, Wang AZ, Lin W. Application of liposomal technologies for delivery of platinum analogs in oncology. International journal of nanomedicine. 2013;8:3309-19.

[14] White SC, Lorigan P, Margison GP, Margison JM, Martin F, Thatcher N, et al. Phase II study of SPI-77 (sterically stabilised liposomal cisplatin) in advanced non-small-cell lung cancer. British journal of cancer. 2006;95:822-8.

[15] Boulikas T, Stathopoulos GP, Volakakis N, Vougiouka M. Systemic Lipoplatin infusion results in preferential tumor uptake in human studies. Anticancer research. 2005;25:3031-9.

[16] Bulbake U, Doppalapudi S, Kommineni N, Khan W. Liposomal Formulations in Clinical Use: An Updated Review. Pharmaceutics. 2017;9.

[17] Maeda H. Tumor-selective delivery of macromolecular drugs via the EPR effect: background and future prospects. Bioconjugate chemistry. 2010;21:797-802.

[18] Prabhakar U, Maeda H, Jain RK, Sevick-Muraca EM, Zamboni W, Farokhzad OC, et al. Challenges and key considerations of the enhanced permeability and retention effect for nanomedicine drug delivery in oncology. Cancer research. 2013;73:2412-7.

[19] Helmlinger G, Yuan F, Dellian M, Jain RK. Interstitial pH and pO2 gradients in solid tumors in vivo: high-resolution measurements reveal a lack of correlation. Nature medicine. 1997;3:177-82.

[20] Vaupel P, Kallinowski F, Okunieff P. Blood flow, oxygen and nutrient supply, and metabolic microenvironment of human tumors: a review. Cancer research. 1989;49:6449-65.

[21] Bandekar A, Sofou S. Floret-shaped solid domains on giant fluid lipid vesicles induced by pH. Langmuir : the ACS journal of surfaces and colloids. 2012;28:4113-22.

[22] Karve S, Bajagur Kempegowda G, Sofou S. Heterogeneous domains and membrane permeability in phosphatidylcholine-phosphatidic acid rigid vesicles as a function of pH and lipid chain mismatch. Langmuir : the ACS journal of surfaces and colloids. 2008;24:5679-88.

[23] Boggs JM. Lipid intermolecular hydrogen bonding: influence on structural organization and membrane function. Biochimica et biophysica acta. 1987;906:353-404.

[24] Jain RK, Stylianopoulos T. Delivering nanomedicine to solid tumors. Nature reviews Clinical oncology. 2010;7:653-64.

[25] Kempegowda GB, Karve S, Bandekar A, Adhikari A, Khaimchayev T, Sofou S. pH-dependent formation of lipid heterogeneities controls surface topography and binding reactivity in functionalized bilayers. Langmuir : the ACS journal of surfaces and colloids. 2009;25:8144-51.

[26] Goodman TT, Ng CP, Pun SH. 3-D tissue culture systems for the evaluation and optimization of nanoparticle-based drug carriers. Bioconjugate chemistry. 2008;19:1951-9.

[27] Mueller-Klieser W. Multicellular spheroids. A review on cellular aggregates in cancer research. Journal of cancer research and clinical oncology. 1987;113:101-22.

[28] Sutherland RM. Cell and environment interactions in tumor microregions: the multicell spheroid model. Science (New York, NY). 1988;240:177-84.

[29] Woo J, Chiu GN, Karlsson G, Wasan E, Ickenstein L, Edwards K, et al. Use of a passive equilibration methodology to encapsulate cisplatin into preformed thermosensitive liposomes. International journal of pharmaceutics. 2008;349:38-46.

[30] Stewart JC. Colorimetric determination of phospholipids with ammonium ferrothiocyanate. Analytical biochemistry. 1980;104:10-4.

[31] Ivascu A, Kubbies M. Rapid Generation of Single-Tumor Spheroids for High-Throughput Cell Function and Toxicity Analysis. Journal of Biomolecular Screening. 2006;11:922-32.

[32] Szebeni J, Bedőcs P, Rozsnyay Z, Weiszhár Z, Urbanics R, Rosivall L, et al. Liposome-induced complement activation and related cardiopulmonary distress in pigs: factors promoting reactogenicity of Doxil and AmBisome. Nanomedicine: Nanotechnology, Biology and Medicine.8:176-84.

[33] Weiswald LB, Bellet D, Dangles-Marie V. Spherical cancer models in tumor biology. Neoplasia (New York, NY). 2015;17:1-15.

[34] Lee H, Fonge H, Hoang B, Reilly RM, Allen C. The effects of particle size and molecular targeting on the intratumoral and subcellular distribution of polymeric nanoparticles. Molecular pharmaceutics. 2010;7:1195-208.

[35] Saif MW, Reardon J. Management of oxaliplatin-induced peripheral neuropathy. Therapeutics and clinical risk management. 2005;1:249-58.

[36] Lebwohl D, Canetta R. Clinical development of platinum complexes in cancer therapy: an historical perspective and an update. European journal of cancer (Oxford, England : 1990). 1998;34:1522-34.

[37] Wang Y, Zhou J, Qiu L, Wang X, Chen L, Liu T, et al. Cisplatin-alginate conjugate liposomes for targeted delivery to EGFR-positive ovarian cancer cells. Biomaterials. 2014;35:4297-309.

[38] Bandekar A, Karve S, Chang MY, Mu Q, Rotolo J, Sofou S. Antitumor efficacy following the intracellular and interstitial release of liposomal doxorubicin. Biomaterials. 2012;33:4345-52.

[39] Rozencweig M, Canetta R, Carter SK. Carboplatin: the clinical evaluation strategy. Cancer treatment reviews. 1985;12 Suppl A:137-44.

[40] Stathopoulos GP, Rigatos SK, Stathopoulos J. Liposomal Cisplatin Dose Escalation for Determining the Maximum Tolerated Dose and Dose-limiting Toxicity: A Phase I Study. Anticancer Research. 2010;30:1317-21.

[41] Karve S, Alaouie A, Zhou Y, Rotolo J, Sofou S. The use of pH-triggered leaky heterogeneities on rigid lipid bilayers to improve intracellular trafficking and therapeutic potential of targeted liposomal immunochemotherapy. Biomaterials. 2009;30:6055-64.

[42] Galluzzi L, Senovilla L, Vitale I, Michels J, Martins I, Kepp O, et al. Molecular mechanisms of cisplatin resistance. Oncogene. 2012;31:1869-83.

[43] Wang D, Lippard SJ. Cellular processing of platinum anticancer drugs. Nat Rev Drug Discov. 2005;4:307-20.

[44] Ishida S, McCormick F, Smith-McCune K, Hanahan D. Enhancing tumor-specific uptake of the anticancer drug cisplatin with a copper chelator. Cancer cell. 2010;17:574-83.

[45] Song I-S, Savaraj N, Siddik ZH, Liu P, Wei Y, Wu CJ, et al. Role of human copper transporter Ctr1 in the transport of platinum-based antitumor agents in cisplatin-sensitive and cisplatin-resistant cells. American Association for Cancer Research. 2004;3:1543-9.

[46] Ovcaricek T, Frkovic SG, Matos E, Mozina B, Borstnar S. Triple negative breast cancer - prognostic factors and survival. Radiology and oncology. 2011;45:46-52.

[47] Telli M. Optimizing Chemotherapy in Triple-Negative Breast Cancer: The Role of Platinum ASCO Educational Book. 2014:e37-e42.

[48] Anders CK, Zagar TM, Carey LA. The management of early-stage and metastatic triple-negative breast cancer: a review. Hematology/oncology clinics of North America. 2013;27:737-49, viii.

[49] Fantini M, Santelmo C, Drudi F, Ridolfi C, Barzotti E, Gianni L, et al. Triple Negative Breast Cancer Treatment: Use of Platinum and Platinum Analogs. Journal of Cancer Therapy. 2012;3:777-81.

[50] Crown J, O'Shaughnessy J, Gullo G. Emerging targeted therapies in triple-negative breast cancer. Annals of Oncology. 2012;23:vi56-vi65.

[51] Oakman C, Viale G, Di Leo A. Management of triple negative breast cancer. The Breast. 2010;19:312-21.

[52] Gelmon K, Dent R, Mackey JR, Laing K, McLeod D, Verma S. Targeting triple-negative breast cancer: optimising therapeutic outcomes. Annals of Oncology. 2012.

[53] van Hennik MB, van der Vijgh WJ, Klein I, Elferink F, Vermorken JB, Winograd B, et al. Comparative pharmacokinetics of cisplatin and three analogues in mice and humans. Cancer research. 1987;47:6297-301.

[54] Minchinton AI, Tannock IF. Drug penetration in solid tumours. Nat Rev Cancer. 2006;6:583-92.

[55] Stras S, Holeran T, Howe A, Sofou S. Interstitial Release of Cisplatin from Triggerable Liposomes Enhances Efficacy Against Triple Negative Breast Cancer Solid Tumor Analogues. Molecular Pharmaceutics. 2016;13:3224-33.

[56] Zhu C, Sempkowski M, Holleran T, Linz T, Bertalan T, Josefsson A, et al. Alpha-particle radiotherapy: For large solid tumors diffusion trumps targeting. Biomaterials. 2017;130:67-75.

[57] Helmlinger G, Yuan F, Dellian M, Jain RK. Interstitial pH and pO2 gradients in solid tumors in vivo: high-resolution measurements reveal a lack of correlation. Nature medicine. 1997;3:177-82.

[58] Vaupel P, Kallinowski F, Okunieff P. Blood Flow, Oxygen and Nutrient Supply, and Metabolic Microenvironment of Human Tumors: A Review. Cancer Res. 1989;49:6449-65.

[59] Bandekar A, Karve S, M.-Y. C, Mu Q, Rotolo J, Sofou S. Antitumor efficacy following the intracellular and interstitial release of liposomal doxorubicin. Biomaterials. 2012;33:4345-52.

[60] Karve S, Alaouie A, Zhou Y, Rotolo J, Sofou S. The use of pH-triggered leaky heterogeneities on rigid lipid bilayers to improve intracellular trafficking and therapeutic potential of targeted liposomal immunochemotherapy. Biomaterials. 2009;30:6055-64.

[61] Karve S, Bajagur Kempegowda G, Sofou S. Heterogeneous domains and membrane permeability in phosphatidylcholine- phosphatidic acid rigid vesicles as a function of pH and lipid chain mismatch Langmuir. 2008;24:5679-88.

[62] Karve S, Bandekar A, Ali MR, Sofou S. The pH-dependent association with cancer cells of tunable functionalized lipid vesicles with encapsulated doxorubicin for high cell-kill selectivity. Biomaterials. 2010;31:4409-16.

[63] Bandekar A, Sofou S. Floret-shaped solid domains on giant fluid lipid vesicles induced by pH. Langmuir. 2012;28:4113-22.

[64] Lieleg O, Baumgärtel RM, Bausch AR. Selective Filtering of Particles by the Extracellular Matrix: An Electrostatic Bandpass. Biophysical Journal.97:1569-77.

[65] Stylianopoulos T, Poh M-Z, Insin N, Bawendi MG, Fukumura D, Munn Lance L, et al. Diffusion of Particles in the Extracellular Matrix: The Effect of Repulsive Electrostatic Interactions. Biophysical Journal. 2010;99:1342-9.

[66] Auguste DT, Armes SP, Brzezinska KR, Deming TJ, Kohn J, Prud'homme RK. pH triggered release of protective poly(ethylene glycol)-b-polycation copolymers from liposomes. Biomaterials. 2006;27:2599-608.

[67] Stras S, Holleran T, Howe A, Sofou S. Interstitial Release of Cisplatin from Triggerable Liposomes Enhances Efficacy against Triple Negative Breast Cancer Solid Tumor Analogues. Molecular pharmaceutics. 2016;13:3224-33.

[68] Stewart JC. Colorimetric determination of phospholipids with ammonium ferrothiocyanate. Anal Biochem. 1980;104:10-4.

[69] Stefansson OA, Villanueva A, Vidal A, Martí L, Esteller M. BRCA1 epigenetic inactivation predicts sensitivity to platinum-based chemotherapy in breast and ovarian cancer. Epigenetics. 2012;7:1225-9.

[70] Iorns E, Drews-Elger K, Ward TM, Dean S, Clarke J, Berry D, et al. A New Mouse Model for the Study of Human Breast Cancer Metastasis. PLoS ONE. 2012;7:e47995.

[71] Mannello F, Qin W, Zhu W, Fabbri L, Tonti G, Sauter E. Nipple aspirate fluids from women with breast cancer contain increased levels of group IIa secretory phospholipase A2. Breast Cancer Research and Treatment. 2008;111:209-18.

[72] Bandekar A, Zhu C, Menzenski MZ, Gomez A, Sempkowski M, Sofou S. Masking and triggered unmasking of targeting ligands on liposomal chemotherapy selectively suppress tumor growth in vivo. Mol Pharm. 2013;10:152-60.

[73] Basu S, Chen W, Tchou J, Mavi A, Cermik T, Czerniecki B, et al. Comparison of triple-negative and estrogen receptor-positive/progesterone receptor-positive/HER2-negative breast carcinoma using quantitative fluorine-18 fluorodeoxyglucose/positron emission tomography imaging parameters. Cancer. 2008;112:995-1000.

[74] Estrella V, Chen T, Lloyd M, Wojtkowiak J, Cornnell HH, Ibrahim-Hashim A, et al. Acidity Generated by the Tumor Microenvironment Drives Local Invasion. Cancer Research. 2013;73:1524-35.

[75] Vaupel P. Tumor microenvironmental physiology and its implications for radiation oncology. Semin Radiat Oncol. 2004;14:198-206.

[76] Gabizon A, Papahadjopoulos D. Liposome formulations with prolonged circulation time in blood and enhanced uptake by tumors. PNAS. 1988;85:6949-53.

[77] Lasic DD, Martin F. Stealth liposomes. Boca Raton, Fla: CRC Press; 1995. p. 289.

[78] Sofou S. Surface-active liposomes for targeted cancer therapy. Nanomed. 2007;2:711-24

[79] Lee H, Shields AF, Siegel BA, Miller KD, Krop I, Ma CX, et al. ^{64}Cu-MM-302 Positron Emission Tomography Quantifies Variability of Enhanced Permeability and Retention of Nanoparticles in Relation to Treatment Response in Patients with Metastatic Breast Cancer. Clinical Cancer Research. 2017;23:4190-202.